The meiotic recombination landscape of *Drosophila virilis* is robust to mitotic damage during hybrid dysgenesis

Lucas W. Hemmer[1†*], Guilherme Dias[2], Brittny Smith[3], Kelley Van Vaerenberghe[1], Ashley Howard[1], Casey M. Bergman[2] and Justin P. Blumenstiel[1]

[1] Department of Ecology and Evolutionary Biology, University of Kansas, Lawrence, KS 66045

[2] Department of Genetics and Institute of Bioinformatics, University of Georgia, Athens, GA 30602

[3] Department of Molecular Biosciences, University of Kansas, Lawrence, KS 66045

[†] Present address: Department of Biology, University of Rochester, Rochester, NY 14627

[*] Corresponding author: lhemmer@ur.rochester.edu

13 **Running title:** *D. virilis* dysgenesis recombination

14 **Key words:** *Drosophila virilis*, hybrid dysgenesis, transposons, meiotic recombination, mitotic

15 recombination

16 **Corresponding author:** Lucas W. Hemmer

17 University of Rochester

18 337 Hutchison Hall, Rochester, NY 14627

19 Phone: 402-920-0456

20 Email: lhemmer@ur.rochester.edu

ABSTRACT

Germline DNA damage is a double-edged sword. Programmed double-strand breaks establish the foundation for meiotic recombination and chromosome segregation. However, double-strand breaks also pose a significant challenge for genome stability. Because of this, meiotic double-strand break formation is tightly regulated. However, natural selection can favor selfish behavior in the germline and transposable elements can cause double-strand breaks independent of the carefully regulated meiotic process. To understand how the regulatory mechanisms of meiotic recombination accommodate unregulated transposition, we have characterized the female recombination landscape in a syndrome of hybrid dysgenesis in *Drosophila virilis*. In this system, a cross between two strains of *D. virilis* with divergent transposable element and piRNA profiles results in germline transposition of diverse transposable elements, reduced fertility, and male recombination. We sought to determine how increased transposition during hybrid dysgenesis might perturb the meiotic recombination landscape. Our results show that the overall frequency and distribution of meiotic recombination is extremely robust to germline transposable element activation. However, we also find that hybrid dysgenesis can result in mitotic recombination within the female germline. Overall, these results show that landscape of meiotic recombination may be insensitive to the DNA damage caused by transposition during early development.

39 **INTRODUCTION**

40 Recombination during meiosis plays a critical role in ensuring proper chromosome segregation
41 (Koehler *et al.* 1996). In addition, meiotic recombination benefits populations since it creates
42 new genotypic combinations that can facilitate adaptation to changing environments (Weismann
43 *et al.* 1904; Burt 2000). While meiosis and sexual reproduction is a conserved process across
44 many eukaryotes, it can be exploited by selfish genetic elements. Transposable elements (TEs)
45 are an example of one such class of selfish genetic element. TEs can increase within the genome,
46 even to the detriment of the host, because fertilization provides a continuous opportunity for TEs
47 to colonize new genomes (Hickey 1982) and recombination uncouples progenitor TEs from the
48 harmful effects of descendant insertions. Upon proliferation, TEs can cause mutation, mis-
49 regulation of gene expression, chromosomal rearrangement, and illegitimate recombination
50 (Kidwell *et al.* 1977; Kazazian *et al.* 1988; Bennetzen 2000; Slotkin *et al.* 2007; Zhang *et al.*
51 2011). Moreover, TEs can activate the DNA damage response within developing germline stem
52 cells and alter stem cell fate (Chen *et al.* 2007; Wylie *et al.* 2014; Tasnim and Kelleher 2018).
53

54 The harmful effects of TEs are especially evident in syndromes of hybrid dysgenesis, where
55 sterility can arise in intraspecific crosses between males carrying TEs and females that lack them
56 (Bingham *et al.* 1982; Bucheton *et al.* 1984; Yannopoulos *et al.* 1987; Lozovskaya *et al.* 1990).
57 Hybrid dysgenesis is the result of TE activation in the absence of maternal repression by PIWI-
58 interacting RNAs (piRNAs) (Aravin *et al.* 2007; Brennecke *et al.* 2008). The piRNA system of
59 genome defense requires maternal deposition of piRNA to successfully silence TEs across
60 generations. The combination of unrecognized TEs introduced to a naive genome *via* sperm and
61 the absence of corresponding piRNAs in the egg results in TE activation and hybrid dysgenesis

62 (Brennecke *et al.* 2008). A unique syndrome of hybrid dysgenesis in *D. virilis* is observed in
63 intraspecific crosses between males of an inducing strain (designated strain 160) and reactive
64 strain females (designated strain 9) (Lozovskaya *et al.* 1990). The primary TE family responsible
65 for inducing dysgenesis remains unknown and sterility appears to be due to the mass activation
66 of several TE families abundant in strain 160 but not strain 9. At least four elements are proposed
67 to contribute significantly to dysgenesis: *Penelope*, *Helena*, *Paris*, and *Polyphemus* (Petrov *et al.*
68 1995; Evgen'ev *et al.* 1997; Vieira *et al.* 1998; Blumenstiel 2014; Funikov *et al.* 2018). In
69 addition, activation of TEs during hybrid dysgenesis also leads to transposition of diverse TEs
70 that are equally abundant between the two strains (Petrov *et al.* 1995).
71
72 The impact of hybrid dysgenesis on recombination during meiosis is an open question. TEs may
73 modulate recombination rates directly since transposition itself can induce illegitimate
74 recombination at the sites of DNA breaks. As a consequence, in the *P-M* system of hybrid
75 dysgenesis in *D. melanogaster*, males undergo recombination (Hiraizumi 1971; Kidwell and
76 Kidwell 1975; Kidwell *et al.* 1977). This is abnormal since meiotic recombination is absent in *D.*
77 *melanogaster* males. However, rates of meiotic recombination induced by *P-M* dysgenesis are
78 typically low, at a rate approximately 2-3% of female meiotic recombination (Preston and Engels
79 1996). *P-M* induced male recombination is usually attributed to an increased rate of mitotic
80 exchange induced by DNA damage (Isackson *et al.* 1981). Many of these recombination events
81 occur near *P* element insertion, require transposase, and are likely the byproduct of *P* element
82 excision events that are repaired from the homolog (McCarron *et al.* 1994; Sved *et al.* 1995;
83 Gray *et al.* 1996; Preston and Engels 1996; Preston *et al.* 1996). The effects of hybrid dysgenesis
84 on female meiotic recombination rates in *D. melanogaster* are less clear. Changes in female

85 recombination rates were not initially observed during *P-M* hybrid dysgenesis (Hiraizumi 1971;
86 Chaboissier *et al.* 1995) but later studies found a slight increase (Kidwell 1977; Broadhead *et al.*
87 1977; Sved *et al.* 1991), often within pericentric heterochromatin. Slightly increased rates of
88 female recombination were also observed within the *I-R* element system, but these were not
89 localized near the centromere (Chaboissier *et al.* 1995). However, others have identified no
90 increase in female recombination rates caused by *P-M* hybrid dysgenesis but, rather, a
91 redistribution towards regions with low recombination and heterochromatic regions near the
92 centromere (Slatko 1978; Hiraizumi 1981). There have been no investigations of how hybrid
93 dysgenesis influences female meiotic recombination in *D. virilis*.
94
95 To determine how transposition influences recombination in *Drosophila* females, fine-scale
96 genetic maps are required. *D. virilis* genetic maps have been obtained only with a limited number
97 of markers which show that the rate of recombination in *D. virilis* is significantly higher than in
98 *D. melanogaster* even though previously estimated rates also differ between studies (Weinstein
99 1920; Gubenko and Evgen'ev 1984; Huttunen *et al.* 2004) (Table 1). Here, we provide the first
100 fine-scale genetic map for *D. virilis* using thousands of genotypic markers. Using this map, we
101 investigate differences in both crossover (CO) frequency and distribution in the hybrid
102 dysgenesis syndrome of *D. virilis*. Interestingly, we find no significant differences in meiotic
103 recombination between genetically identical dysgenic and non-dysgenic female progeny. Instead,
104 we find a strong signature of mitotic recombination that is likely derived from transposition
105 events in the early germline. Thus, at least in *D. virilis*, meiotic recombination is remarkably
106 robust to TE activation during hybrid dysgenesis. This suggests that the effects of DNA damage

107 during early development are not sufficient to trigger changes in the control of recombination
108 later during meiosis.
109

110 **MATERIALS AND METHODS**

111 **Fly Stocks and crosses**

112 The hybrid dysgenesis syndrome in *D. virilis* is observed in crosses between reactive strain 9
113 females and inducer strain 160 males (Lozovskaya *et al.* 1990; Erwin *et al.* 2015). The study was
114 performed in two stages. A smaller pilot study was performed, followed by a larger second study
115 that incorporated additional optimization. We observed no differences between these two
116 experiments, so we combined results for final analysis (see below). For both experiments, each
117 strain and all subsequent crosses were maintained on standard media at 25°C. Prior to creating
118 dysgenic and non-dysgenic hybrids, strain 160 and strain 9 were each inbred for 10 generations
119 by single sib-pair matings. For each direction of the cross, approximately 20 4- to 6-day old
120 virgin females of one strain and 20 2- to 10-day old males of the other strain were crossed *en*
121 *masse* in bottles for six days. Strain 160 males crossed with strain 9 females induce dysgenesis in
122 the F1 generation while the reciprocal cross yields non-dysgenic F1 progeny. Reciprocal crosses
123 yield F1 files with identical genetic backgrounds, with the exception of the mitochondrial
124 genome. By comparing the recombination landscape between F1 females with identical nuclear
125 genotypes, we obtain a robust analysis of how hybrid dysgenesis influences recombination that
126 effectively controls for genetic background. Individual virgin F1 females, four days post-
127 emergence, were backcrossed in single vials to two or three 2- to 10-day old strain 9 males and
128 maintained in vials for six days. Some non-dysgenic females were only allowed to lay for four or
129 five days due to their high fertility to prevent vial crowding. Because fertility was low in

130 dysgenic females, and to increase sample size of progeny within cohorts in the second
131 experiment, a second brood was obtained from some dysgenic F1 females by transferring to
132 another vial after ten days. These females were allowed to lay for an additional four days. We
133 found no difference in recombination between first and second broods (see below), so results
134 were combined across broods. Female backcross progeny (BC1) were collected once per day and
135 immediately frozen at -20°C. Between 12 and 20 sisters from each non-dysgenic F1 female was
136 collected as a sibship. All female progeny of the dysgenic F1 backcrosses were collected.
137
138 There is a high amount of variation in fecundity in dysgenic females. Some females are
139 completely sterile, others have only reduced fecundity and some even have high numbers of
140 progeny. One approach to analyzing the effects of dysgenesis on recombination would be to
141 sample only single daughters from each F1 female. However, this approach would not allow for
142 the discovery of recombination events arising as clusters within the germline. Therefore, we
143 elected to sequence cohorts of BC1 sisters, balancing our sequencing across cohorts with
144 different levels of fecundity. To determine if there might be an effect of fecundity on
145 recombination, all male and female BC1 progeny across the two broods from the second larger
146 experiment were counted to estimate the fecundity of the F1 mother. In some cases, dysgenic F1
147 females escape the effects of dysgenesis completely and produce as many progeny as non-
148 dysgenic females. For these dysgenic F1 females, designated high fecundity, approximately 40
149 BC1 female progeny were subjected to recombination analysis by sequencing. Progeny produced
150 by the low fecundity F1 dysgenic females were collected with cohort sizes ranging from one to
151 40 sisters. By sampling larger cohorts from high fecundity F1 dysgenic females, we sought to
152 identify clustered recombination events derived within the germline of single females. Power to

153 detect these events among a small cohort of sisters is low. By examining recombination in both
154 high fecundity and low fecundity dysgenic females, we also obtained an additional comparison
155 in the analysis of recombination landscapes between two outcomes of TE activation: TE
156 activation with strong deleterious effects on fertility versus TE activation with no observable
157 negative effects on fertility. For a full description of sampling, see Table S1.
158
159 **DNA extraction, library preparation, and Illumina sequencing**
160 Sequencing libraries were prepared in two batches using different protocols. The first batch
161 included 192 samples and library preparations were performed following the protocol outlined in
162 Andolfatto *et al.* (2011) with minor modifications. Single flies were placed into a U-bottom
163 polypropylene 96-well plate with lysis buffer and 3.5 mm steel grinding balls (BioSpec) then
164 homogenized with a MiniBeadBeater-96 at 2,100 rpm for 45 seconds. DNA extractions on
165 homogenized tissue were performed with the Agencourt DNAdvance Genomic DNA Isolation
166 Kit (Beckman Coulter) following the Insect Tissue Protocol. DNA quantification was spot
167 checked on some samples and estimated to average 1-2 ng/µl. For each sample, 10 µl of genomic
168 DNA was digested with 3.3 U of MseI in 20 µls of reaction volume for four hours at 37°C,
169 followed by heat inactivation at 65°C for 20 min. FC1 and FC2 adaptors (Andolfatto *et al.* 2011)
170 (Table S2-S3) were ligated to the digested DNA with 1 U of T4 DNA ligase (New England
171 Biolabs) in 50 µl of reaction volume at 16°C for 5 h and inactivated at 65°C for 10 minutes. The
172 samples were pooled and concentrated using isopropanol precipitation (1/10 vol NaOAc at pH
173 5.2, 1 vol of 100% isopropanol, and 1 µl glycogen). The library was resuspended in 125 µl of 1X
174 Tris-EDTA (pH 8). Adapter dimers were removed with 1.5X vol AMPure XP Beads (Agencourt)
175 and ligated products were resuspended in 32 µl of 1X Tris-EDTA (pH 8). 200-400 bp DNA

176 fragments were selected using a BluePippin (Sage Science). Size-selected fragments were
177 cleaned using 2X vol of AMPure XP beads and resuspended 20 µl of 1X elution buffer (10 µM
178 Tris, pH 8). Libraries were quantified using a Qubit fluorometer before an 18-cycle PCR
179 amplification on bar-coded fragments with Phusion high-fidelity PCR Kit (New England
180 Biolabs). The PCR products were cleaned using 1X vol of AMPure XP Beads.
181
182 For the larger second batch (768 samples), sequencing libraries were constructed with an
183 optimized rapid DNA extraction protocol that uses an in-house Tn5 transposase similar to the
184 procedure outlined in Picelli *et al.* (2014). DNA was extracted using the *Quick*-DNA 96 kit
185 (Zymo) and 1-2 ng of DNA was tagmented with Tn5 transposase stored at a concentration of 1.6
186 mg/ml with pre-annealed oligonucleotides. Tagmentation was performed in 20 µl reaction
187 volumes containing 2 µl of 5X TAPS-DMF buffer (50 mM TAPS-NaOH, 25 mM $MgCl_2$ (pH
188 8.5), 50% v/v DMF) and 2 µl of 5x TAPS-PEG buffer (50 mM TAPS-NaOH, 25 mM $MgCl_2$ (pH
189 8.5), 60% v/v PEG 8000). Samples were incubated at 55°C for 7 min then rapidly lowered to a
190 holding temperature of 10°C. Reactions were inactivated with 5 µl of 0.2% SDS followed by an
191 additional incubation at 55°C for 7 min. PCR-based barcoding was performed on 2.5 ul of
192 sample tagmentation volumes using the KAPA HiFi HotStart ReadyMix PCR Kit (Thermo
193 Fisher Scientific), 1 µl of 4 µM Index 1 (i7) primers (Table S4), and 1 µl of 4 µM Index 2 (i5)
194 primers (Table S5) in 9 µl of reaction volume. The PCR thermocycling conditions were: 3 min at
195 72°C, 2 min 45 sec at 98°C, followed by 14 cycles of 98°C for 15 sec, 62°C for 30 sec, 72°C for
196 1 min 30 sec. PCR-amplified samples were pooled and the pooled samples were cleaned using
197 0.8 X vol AMPure XP Beads. We size-selected DNA fragments 250-400 bp from the pooled
198 sample on a BluePippin and cleaned using 1X vol of AMPure XP Beads.

199

200 All libraries were sequenced at the University of Kansas Genomics Core on an Illumina HiSeq
201 2500 Sequencer with 100 bp single-end sequencing. The first 192 samples were sequenced on
202 two lanes using the Rapid-Run Mode while the Tn5-produced libraries were sequenced on two
203 lanes using the High-Output Mode (summary of the output is in File S2).

204

205 **DNA extraction, library preparation, Pacbio sequencing and assembly**

206 PacBio sequencing was performed on strain 160 after 10 generations of single-sib mating
207 followed by re-validation for induction of dysgenesis. Females collected for DNA extraction
208 were allowed to eclose over 10 days, aged for two additional days, starved for 12 hours to
209 evacuate the gut, then immediately frozen in liquid nitrogen. 500 mg of whole flies were then
210 used for DNA extraction with Blood Cell and Culture Midi Kit (Qiagen) (Chakraborty *et al.*
211 2016). The mortar was pre-chilled with liquid nitrogen prior to grinding and the resulting fine
212 powder was directly transferred into Buffer G2. DNA extraction was performed across 5
213 columns, using a total of 47.5 mls G2, 190 µl RNAse A (100 mg/ml) and 1.25 ml of Protease
214 from the Qiagen Kit. 50 mls were placed in a 50°C shaker overnight. After overnight incubation,
215 debris was spun down and poured onto column. The elution was performed according to
216 manufacturer's instructions and precipitated with 0.7 volumes of isopropanol, followed by
217 spooling with a glass rod and resuspending in 100ul EB Buffer. The final DNA concentration
218 was estimated with a Qubit to be 843 ng/ul, yielding approximately 85 µg. PacBio sequencing
219 was performed by the University of Michigan DNA Sequencing Core.

220

221 Purified strain 160 DNA was used to generate PacBio SMRTbell libraries using the protocol:
222 Procedure & Checklist 20 kb Template Preparation using BluePippin Size Selection. Briefly,
223 approximately 10 µg of template was sheared using Covaris g-TUBES to obtain a 20-25 Kb
224 target length. Sheared DNA was purified using pre-washed AMPureXP beads, analyzed for size
225 and concentration, then treated with Exo VII to remove single stranded DNA, followed by DNA
226 damage and end repair. End repaired DNA was then blunt ligated to adaptors to form SMRTbells
227 and treated with Exo VII plus Exo III to remove any fragments that lack adaptors on both ends.
228 SMRTbells were purified using pre-washed AMPureXP beads, analyzed for size and
229 concentration, then run through a Sage Scientific Blue Pippin instrument with 0.75% agarose
230 dye-free cassette and S1 external marker to remove templates smaller than 10 kb. The PacBio
231 Binding Calculator was used to determine conditions to anneal primers to SMRTbells and bind
232 DNA polymerase (P6/C4 chemistry) to form SMRTbell-primer-polymerase complexes.
233 Complexes were bound to Magbeads and washed to remove unbound template and other
234 contaminants. Purified complexes with an added Pacific Biosciences internal control were loaded
235 on a PacBio RS II instrument and run using the MagBead-OCPW protocol. The resulting library
236 was sequenced on 21 SMRT cells with a movie time of 360 minutes per SMRT cell, totaling
237 ~80-fold coverage of the estimated ~380 Mb *D. virilis* genome (Bosco *et al.* 2007).
238
239 Assembly of the PacBio reads was performed using Canu v1.5 with default settings (Koren *et al.*
240 2017). Canu performs read correction on the 40x longest reads based on the genomeSize
241 parameter. This parameter was set to 200 Mb after analyzing the read size distribution to avoid
242 including shorter reads that could result in deterioration of assembly quality. The raw PacBio
243 reads were aligned back to the Canu assembly with pbmm2 v1.0.0. and the assembly was

244 polished with Arrow using gcpp v0.01.e12a6d6. PacBio polishing software were downloaded as
245 part of the pb-assembly metapackage v0.0.6 from bioconda
246 (https://github.com/PacificBiosciences/pb-assembly). A second round of polishing was
247 performed after aligning Illumina reads from strain 160 (SRR1200631, Erwin *et al.* 2015) with
248 BWA-MEM v0.7.17-r1188 (Li 2013) and correcting errors with Pilon v1.22 (Walker *et al.*
249 2014). Since *D. virilis* strain 160 is largely colinear with the current *D. virilis* reference genome
250 (strain 15010-1051.87; *Drosophila* 12 Genomes Consortium 2007), we performed reference-
251 based scaffolding of the strain 160 PacBio assembly using RaGOO v1.1 (Alonge *et al.* 2019).
252 RaGOO performs scaffolding and correction of potential misassemblies by aligning *de novo*
253 assemblies to a reference genome and breaking chimeric contigs where necessary. For the
254 reference, we used an updated version of the SNP-corrected reference genome for strain 160
255 generated in Erwin *et al*. (2015) that incorporates the chromosome mapping data generated by
256 Schaeffer *et al.* (2008; see below). General assembly statistics were analyzed with QUAST
257 v5.0.2 (https://github.com/ablab/quast, commit 67a1136, Gurevich *et al*. 2013). Assembly
258 completeness was assessed by searching for highly conserved orthologs with BUSCO v3.0.2
259 (Simão *et al*. 2015) using the Diptera ortholog gene set from OrthoDB v9 (Zdobnov *et al.* 2016).
260 Assembly statistics are available in Table S6. Coordinates of the mitotic CO clusters (see
261 methods below) were lifted over to the final version of the PacBio assembly using minimap2
262 2.16-r922 (Li 2018).
263
264 **Annotation of genome resources**
265 Illumina-based reference genomes for strains 9 and 160 (Erwin *et al.* 2015) based on the original
266 Sanger shotgun sequence assembly of *D. virilis* (*Drosophila* 12 Genomes Consortium 2007)

267 were annotated with the most up-to-date gff file for *D. virilis* (v1.6 Flybase, Gramates *et al.*
268 2017) using Maker v3.31.9 on default settings (Cantarel *et al.* 2008). Due to errors in the original
269 reference assembly, genome region 33,464,439-35,498,860 on Chromosome 2 was excluded and
270 genome region 22,673,797-24,330,628 on Chromosome 5 was placed at position 3,761,384 on
271 the same chromosome. Thus, previous strain-specific reference genomes (Erwin *et al.* 2015)
272 were adjusted for two mis-assemblies and updated as '_2' (strain 9, File S3; strain 160, File S4).
273 TE annotations for Illumina-based reference genomes were obtained using RepeatMasker v4.06
274 (Tarailo-Graovac and Chen 2009) with the custom TE library from Erwin *et al.* (2015). TE
275 annotation of the strain 160 PacBio assembly was also obtained using RepeatMasker with the
276 custom TE library from Erwin *et al.* (2015).
277
278 **Crossover quantification**
279 Illumina FASTQ files were parsed according to barcode sequences and trimmed by the
280 University of Kansas Genomics Core facility. The FASTQ files were mapped to the Illumina-
281 based reference genomes for strains 9 and 160 using the multiplex shotgun genotyping (MSG:
282 https://github.com/JaneliaSciComp/msg) bioinformatic pipeline for identifying reliable markers
283 and determining ancestry at those markers using a hidden Markov model (HMM) v0.1
284 (Andolfatto *et al.* 2011). Briefly, reads were mapped with BWA aln to the strain 9 and 160
285 parental reference _2 files. Output files were used for HMM determination of ancestry along the
286 length of the chromosomal segments (see control file, File S5, for settings). The MSG pipeline
287 provides both ancestry probability calls and CO positions, along with an estimate of the
288 boundaries for CO positions. Samples with fewer than 10,000 reads were discarded. Double COs
289 less than 750 kb apart were discarded as these events were considered unlikely. We observed that

290 reads mapping to regions near the telomere and centromere often predicted the same genotype
291 across all samples. In principle, this could be driven by segregation distortion. However, these
292 regions also showed low density for uniquely mapped reads. In addition, segregation distortion
293 for these regions would drive distortion of linked flanking markers, which we did not see.
294 Therefore, we considered these regions problematic and removed them from the analysis. COs
295 located within 500 kb of the telomere of the X and 4th chromosome and COs within 700 kb on
296 the 2nd, 3rd, and 5th chromosomes were removed. COs near the centromeres were also removed
297 as follows: within 3.5 Mb on the X chromosome, within 1.1 Mb on the 2nd chromosome, within
298 1.5 Mb on the 3rd chromosome, within 2.4 Mb on the 4th chromosome, and 2.3 Mb on the 5th
299 chromosome. The 6th chromosome (corresponding to the 4th in *D. melanogaster*) was also
300 removed from analysis. In addition, we performed additional manual curation of COs to remove
301 calls that appeared incorrect. For example, double COs that were spaced closely in samples with
302 lower numbers of reads and based on ancestry probabilities that were less than 0.9
303
304 **Data analysis**
305 CO outputs from the MSG pipeline were analyzed with R Version 3.4.2 (R Core Team 2017).
306 Ancestry probability outputs were used in the R/qtl package (Broman *et al.* 2003) to construct
307 genetic maps and calculate interference using the Housworth Stahl model (Housworth and Stahl
308 2003) using the xoi package (Broman and Kwak, Version 0.67-4). We used the lme4 (Bates *et al.*
309 2015) and lsmeans (Lenth 2016) packages for mixed-model testing of CO events in BC1
310 progeny. The model construction was performed using the glmer() and glm() functions to test the
311 random effects of F1 female and fecundity of the F1 female and the fixed effects of dysgenesis
312 and batches. Fecundity estimates obtained from dysgenic crosses in the second experiment were

313 first used to determine if fecundity had an effect on total CO count. We found that fecundity had
314 no effect on CO count (χ^2_1= 2.02, p = 0.155) and excluded it from the final model.
315
316 The model for how these effects predict total CO numbers in R was as follows:
317
318 glmer(CO.sum ~ batch (fixed) * dys.nondys (fixed) * parent (random),
319 family=poisson(link=log))
320
321 We used likelihood ratio tests to determine the significance of each effect on variance in total CO
322 number. We used the Biostrings R package (Pagès et al. 2017) to analyze genomic sequences for
323 correlations between genomic features and recombination. Figures were constructed using
324 ggplot2 (Wickham 2016).
325
326 **Analysis of mitotic recombination**
327 Mitotic (or pre-meiotic) recombination is identified by the presence of crossovers that are
328 common among the progeny of a single parent. These are commonly designated as
329 recombination clusters and are distinct from hotspots because they are found only within cohorts
330 of siblings. Clusters indicating germline mitotic recombination were identified as COs in four or
331 more progeny of a single F1 mother within a 100 kb span. Since the fecundity effects of hybrid
332 dysgenesis are highly variable, there was imbalance in progeny counts from dysgenic and non-
333 dysgenic backcrosses. It was therefore necessary to account for this variation in the estimation of
334 rates of mitotic recombination. This was achieved using a likelihood approach to determine if
335 rates of mitotic cluster formation (α) within the germline and the frequency of mitotic

recombination within cohorts (β, conditional upon cluster formation) differed between dysgenic and non-dysgenic parents. Only one mitotic cluster was ever observed per single chromosome so rate estimate was performed on a per chromosome basis. The probability of not observing a cluster event (on a given chromosome) is given by the probability that a mitotic recombination event does not occur in the germline (1-α) plus the probability that a mitotic recombination event does occur (α) but is not observed among the sampled progeny:

$$P_{ClusterNotObs} = (1 - \alpha) + \alpha \times P_{ClusterNotSampled|ClusterOccurred}$$

Conditional on mitotic recombination occurring, the probability that it was not observed is equal to the probability that three or fewer progeny within the cohort inherit the recombinant chromatid from the mother. This is given with the binomial probability distribution where β is the frequency of recombinant chromosomes transmitted by the mother with the mitotic event:

$$P_{ClusterNotSampled|ClusterOccurred} = \sum_{x=0}^{3} \frac{N!}{x!\,(N-x)!} \beta^{x} (1-\beta)^{N-x}$$

where *N* is the total number of progeny in the cohort, β and is the frequency of progeny that inherit the recombinant chromosome. Therefore, parents with three or fewer progeny have $P_{ClusterNotSample|ClusterOccurred} = 1$ under our criteria.

When a cluster event is observed, the probability of *x* progeny with the recombinant chromosome is given by:

$$P(x) = \frac{N!}{x!\,(N-x)!}\beta^{x}(1-\beta)^{N-x}$$

Overall, the probability that a cluster is observed at a given frequency within a cohort is equal to the probability that mitotic recombination happened (α) multiplied by the probability that it is observed at a given frequency, conditional on it having happened:

$$P_{ClusterObserved} = \alpha \times \frac{N!}{x!\,(N-x)!}\beta^{x}(1-\beta)^{N-x}$$

The full likelihood of the data is thus given by:

$$L(Data) = \prod_{i=1}^{m} P_{i.ClusterNotObserved} \prod_{j=1}^{n} P_{j.ClusterObserved}$$

where *i* is index of mothers without an observed mitotic cluster and *j* as the index of mothers whose progeny indicate a mitotic cluster. Taking the logarithm of our likelihood equation gives

$$\log\big(L(Data)\big) = \sum_{i=1}^{m} P_{i.ClusterNotObserved} + \sum_{j=1}^{n} P_{j.ClusterObserved}$$

Mitotic recombination was only ever observed on the X and 3rd chromosomes so a combined rate was only estimated for these two chromosomes. To estimate rates of mitotic recombination across dysgenic and non-dysgenic females, we used the Python module Scipy to maximize the log-likelihood of the data based on α and β. Nested likelihood ratio tests were used to determine

380 whether there was support for unique values of α or β in dysgenic or non-dysgenic females. Two
381 three-parameter models were used with distinct cluster formation rates for dysgenic (D) and non-
382 dysgenic (ND) females (α_D, α_{ND}, β) and, reciprocally, separate frequencies of transmission of the
383 recombinant chromatid (α, β_D, β_{ND}). We also used as a four-parameter model with individual
384 estimates for the dysgenic and non-dysgenic mothers (α_D, α_{ND}, β_D, β_{ND}). 95% confidence intervals
385 (95% CIs) for parameter estimates were obtained by determining parameter values with
386 likelihood scores two log-likelihood units from the ML estimate with other maximum likelihood
387 estimated parameters fixed. We tested if models were significantly improved with the inclusion
388 of additional parameters with a likelihood ratio test (LRT) and a chi-squared distribution with
389 one degree of freedom for every additional parameter estimated. The Python script for the
390 maximum likelihood analysis of the mitotic recombination rates is in File S6.
391
392 **Data availability**
393 All of the de-multiplexed Illumina sequencing reads from BC1 progeny, PacBio reads for strain
394 160, and the strain 160 PacBio assembly generated in this study are available at the National
395 Center for Biotechnology Information under accession PRJNA553533. Supplemental files are
396 available at FigShare.
397
398 **RESULTS**
399 **Crossover detection by sequencing**
400 To identify recombination events in reciprocal F1 dysgenic and non-dysgenic progeny, F1
401 females were backcrossed to reactive strain 9. By sequencing backcross (BC1) progeny, we
402 identified the recombination events that occurred under the dysgenic and non-dysgenic condition

403 in the germline of F1 females. F1 dysgenic and non-dysgenic female progeny have identical
404 nuclear genotypes, which enables a controlled comparison of the effects of TE mobilization on
405 the recombination landscape. In total, 828 BC1 female progeny were sequenced at sufficient
406 depth to map recombination breakpoints; 132 samples had fewer than 10,000 reads and were not
407 included in our analysis. 275 BC1 progeny were sequenced from 20 F1 non-dysgenic females,
408 311 BC1 progeny were sequenced from 66 low fecundity F1 dysgenic females, and 242 BC1
409 progeny were sequenced from seven high fecundity F1 dysgenic females. Across all samples, the
410 MSG pipeline identified a total of 1,150,592 quality-filtered SNPs between the two parental
411 genomes with an average of distance of 136 bp between SNPs. The MSG HMM uses relative
412 mapping abundance of reads that are uniquely derived from one of the two parental strains.
413 Using this information, combined with the crossing scheme, it provides genotype probabilities
414 for each SNP. For each sample, and at each SNP, the HMM provided a genotype probability of
415 the BC1 progeny sample being either homozygous for strain 9 (the strain that the F1 progeny
416 were backcrossed to) or heterozygous. CO breakpoint intervals were then defined based on local
417 genotype probability calls that switch from greater than 95% to less than 5% along the
418 chromosome. The median CO breakpoint interval calculated by the MSG HMM was
419 approximately 18 kb and 84% of all COs localized within a span of 50 kb or less. Seventeen CO
420 breakpoint intervals were approximately ~ 1 Mb but those were in samples with low read counts
421 near the 10,000 read cutoff for samples allowed in the analysis.
422
423 **A high-resolution genetic map of *D. virilis***
424 Previous studies indicate that the genetic map of *D. virilis* is approximately three times larger
425 than the genetic map of *D. melanogaster* (Gubenko and Evgen'ev 1984; Huttunen *et al.* 2004).

426 Critically, the map lengths obtained in those two studies are quite different (Table 1), perhaps
427 due to a limited number of genetic markers available. Our combined sample has a sufficient
428 density of markers to provide the first high-resolution recombination map for *D. virilis*.
429 Combining results from all samples to construct our map was reasonable, since the effects of
430 dysgenesis were non-significant (see below).
431
432 The total genetic map length of *D. virilis* estimated in our combined sample is 732 cM
433 (centiMorgans) or 2.5 times longer than the genetic map length of *D. melanogaster* (Comeron *et*
434 *al.* 2012) (Table 1). The genetic map length estimated in the current study is more than 100 cM
435 shorter than the first detailed genetic map of *D. virilis* (Gubenko and Evgen'ev 1984) (Table 1).
436 This may be partly explained by our stringent exclusion of problematic genomic regions.
437 However, comparing chromosomes that were characterized in all three studies (2, 3, 4, and 5),
438 our estimate for cM is within or very close to the upper estimate of the two prior studies. In
439 addition, our cM estimates were more uniform across the chromosomes, which are all fairly
440 similar in physical length. As expected, the genetic map length of each chromosome in our study
441 correlates with physical length (R^2= 0.851, p = 0.025). There is no significant correlation in the
442 two prior studies (R^2= 0.079, p = 0.72, Huttunen *et al.* 2004; R^2= 0.358, p = 0.28, Gubenko and
443 Evgen'ev 1984, excluding the 6th chromosome). The differences in recombination rates between
444 *D. virilis* and *D. melanogaster* might appear explained due to their differences in genome size.
445 The estimated genome size of *D. virilis* is roughly twice the size of the *D. melanogaster* genome,
446 (404 vs 201 Mb, Bosco *et al.* 2007). Thus, across the entire genome, the average rate of
447 recombination in *D. virilis* is 1.8 cM/Mb and similar to the average recombination rate of 1.4
448 cM/Mb in *D. melanogaster*. However, close to half of the *D. virilis* genome is comprised of

449 satellite DNA, with large expanses of centromeric heterochromatin where little or no crossing
450 over takes place (Gall and Atherton 1974; Bosco *et al.* 2007). Thus, the *D. virilis* assembly of
451 euchromatin, where most COs take place, is 206 Mb in length. Accounting for just euchromatic
452 regions in both species, the average rate of recombination in euchromatin in *D. virilis* is twice as
453 high as *D. melanogaster* based on euchromatic assembly genome size (3.5 cM/Mb vs. 1.8
454 cM/Mb). One possible reason for a higher rate of recombination in *D. virilis* may be the fact that
455 pericentric heterochromatin comprised of satellite DNA may shield the chromosomes arms from
456 the suppressive centromere effect (Hartmann *et al.* 2019).
457
458 Interference reduces the probability of an additional CO in proximity to other COs. We
459 calculated interference in *D. virilis* using the Housworth-Stahl model to calculate *nu*, a unitless
460 measure of interference, with a maximum likelihood function based on intercrossover distances
461 (Housworth and Stahl 2003). If COs are not subject to interference, intercrossover distances are
462 Poisson distributed and *nu* is equal to one (Broman and Weber 2000). *nu* values greater than one
463 are observed when COs are spaced more evenly than expected under a Poisson process. Each
464 chromosome in *D. virilis* has detectable interference between COs with an average *nu* ~ 3 (Table
465 2). The Houseworth-Stahl model also estimates the percentage of COs produced through an
466 alternative pathway not subject to interference as the escape parameter *P* (de los Santos *et al.*
467 2003). Less than 1% of the COs in our study are estimated to be produced through the alternative
468 CO pathway (Table 2). In contrast to interference, assurance is the recombination control
469 mechanism that maintains a minimal number of COs on each chromosome to ensure proper
470 chromosome segregation during meiosis. In the absence of CO assurance and interference, the
471 distribution of COs should resemble a Poisson distribution with variance in CO number equal to

472 the mean. We find the CO mean and variance are not equal (7.3 and 4.9, respectively) and the
473 distribution of CO counts is significantly different from a Poisson distribution ($\chi^2 = 53.6$, $p =$
474 5.74E-08). Moreover, *D. virilis* has a higher than expected frequency of individuals with CO
475 numbers close to the mean (5-8 COs) and a lower than expected frequency of extreme CO
476 numbers (Figure S1). This indicates the collective action of CO assurance and interference.
477
478 In many organisms, the total number of COs between markers in a single tetrad is unobservable
479 because COs are typically detected using random spore analysis based on only one of the four
480 chromatids resulting from meiosis. In contrast, tetrad analysis uses the number of COs for each
481 of the four meiotic products to estimate the frequency of non-exchange tetrads (E_0), single-
482 exchange tetrads (E_1), or multiple-exchange tetrads (E_n) (Weinstein 1918). We used the
483 Weinstein method to estimate the frequency of E_0 tetrads for each chromosome in *D. virilis*. The
484 X chromosome and third chromosome E_0 tetrad frequencies were estimated at 1.2% and 2.1%
485 respectively. These calculated E_0 tetrad frequencies in *D. virilis* are lower in comparison to *D.*
486 *melanogaster*, previously estimated to be 5-10% (Zwick *et al.* 1999; Hughes *et al.* 2018).
487 However, the Weinstein method indicated negative E_0 tetrad frequencies ranging from -2.6% to -
488 3.9% for the second, fourth, and fifth chromosomes. Negative values were also sometimes
489 obtained for other exchange class frequencies (Table S7). Negative tetrad frequencies are a
490 drawback to using the classic Weinstein method (Zwick *et al.* 1999). Nonetheless, these results
491 indicate that there are many fewer non-exchange tetrads in *D. virilis* compared to *D.*
492 *melanogaster*, consistent with the higher estimated rate of recombination per Mb in *D. virilis*.
493

494 Recombination rates are often correlated with certain sequence features, such as GC content,
495 simple motifs, and nucleotide polymorphism (Begun and Aquadro 1992; Kong *et al.* 2002;
496 Comeron *et al.* 2012). In *D. virilis*, recombination rates appear to be weakly correlated with GC
497 content and gene density as not all chromosomes show significant correlations with either
498 sequence parameter (Table 3). This may be due to unusual patterns of recombination along the
499 length of the chromosome (discussed later). Simple repeats and SNP density between the two
500 strains show significant positive correlations with recombination rate on all chromosomes even
501 after removal of non-recombining regions. Nucleotide diversity is frequently correlated with
502 recombination rates (Begun and Aquadro 1992; Kong *et al.* 2002) and the strong correlation
503 between SNP density and recombination in our data is consistent with this pattern (Figure S2).
504 TE density shows a strong negative correlation with recombination rate but this becomes weaker
505 when non-recombining regions are removed (Table 3, Figure S2). The similar pattern of weak
506 correlation between TE density and recombination when regions without recombination are
507 removed is also seen in *D. melanogaster* (Rizzon *et al.* 2002), where TEs mostly accumulate in
508 non-recombining pericentromeric heterochromatin (Bartolomé *et al.* 2002; Bergman *et al.* 2006).
509

510 **No modulation of recombination rates during hybrid dysgenesis**

511 To compare recombination rates in dysgenic and non-dysgenic females, we constructed a full
512 mixed-effects likelihood model using the lme4 R package (Bates et al. 2015). The direction of
513 the cross (dysgenic vs. non-dysgenic) and F1 collection batch (pilot vs. second experiment) were
514 treated as fixed effects; the F1 female of origin was treated as a random effect. In the full model,
515 we find no difference in the total number of COs between the pilot and second experiment (χ^2_1 =
516 0.10, p = 0.755). This suggests that there were no effects of library construction procedure and

517 justifies combining data sets. Likewise, no effect was found for fecundity in dysgenic flies on
518 CO numbers ($\chi^2_1 = 2.02$, $p = 0.155$). Importantly, dysgenesis did not have a significant effect on
519 total CO numbers ($\chi^2_1 = 0.45$, $p = 0.506$) with nearly identical means in CO number between
520 dysgenic and non-dysgenic progeny (Figure 1A). There was a marginal interaction between
521 dysgenesis and batch ($\chi^2_1 = 3.17$, $p = 0.075$), but this appears driven by a single high fecundity
522 dysgenic F1. This F1 female, designated 701, revealed a significantly larger mean CO number
523 than the other high fecundity dysgenic females (8.3 COs, least squares mean contrast, $p = 0.021$,
524 Figure 1B). Without the 701 female, the interaction between dysgenesis and batch is non-existent
525 ($\chi^2_1 = 0.06$, $p = 0.803$). Overall, full model revealed that the identity of the female had minimal
526 effect on CO number (variance < 0.0001).
527
528 The higher recombination rate per Mb in *D. virilis* in comparison to *D. melanogaster* is due to a
529 higher number of COs on each chromosome. In *D. melanogaster*, chromosome arms typically
530 have zero, one, or two COs with three COs on a single chromosome arm being rare (Miller *et al.*
531 2016). In contrast, a chromosome with three or more COs is common in *D. virilis*, in both
532 dysgenic and non-dysgenic directions of the cross. Chromosomes with five COs were also
533 observed (Figure 2). CO counts per chromosome were highly similar between the progeny of
534 dysgenic and non-dysgenic F1 females ($\chi^2_4 = 0.529$, $p = 0.97$). Likewise, there was also no
535 difference between dysgenic mothers if they were high fecundity ($\chi^2_4 = 3.70$, $p = 0.45$) or low
536 fecundity ($\chi^2_4 = 3.45$, $p = 0.49$). Since per chromosome CO counts provide the data for tetrad
537 analysis, these results indicate that dysgenesis does not modulate tetrad exchange class
538 frequency.
539

540 We also examined the distribution of recombination events along the length of each chromosome
541 between non-dysgenic flies, high fecundity dysgenic flies, and low fecundity dysgenic flies.
542 There were no major changes in the distribution of recombination along the length of the
543 chromosomes (Figure 3). The chromosomal recombination rates between all three groups are
544 strongly correlated (Table S8). Interference plays a role in determining CO positioning.
545 Therefore, we determined whether interference was altered by dysgenesis by comparing the
546 distribution of distances between crossovers identified in the progeny of dysgenic and non-
547 dysgenic flies. We found no differences in the distribution of crossovers for any chromosome
548 (Mann-Whitney U test, $p > 0.5$). Overall, we find no differences in the recombination landscape
549 between dysgenic and non-dysgenic F1 mothers in *D. virilis* at the global level. This suggests
550 there is little to no feedback between putative activation of the DNA damage response during
551 dysgenesis in *D. virilis* and the modulation of meiotic recombination.
552
553 **A signature of early DNA damage and mitotic crossing over in dysgenesis**
554 Despite observing no significant effect of dysgenesis on meiotic recombination rates, we
555 observed several genomic regions that exhibited a much higher apparent number of COs during
556 hybrid dysgenesis. For example, within a 500 kb region on the third chromosome, the apparent
557 recombination rate was 26 cM/Mb, nearly twice as high as any other interval within the genome
558 (Figure 3C, within the circled region). 32 COs were identified as arising from dysgenic F1
559 females compared to a single CO identified from non-dysgenic mothers. The COs in this interval
560 provided evidence for a mitotic recombination cluster because the majority (28/32) were
561 identified in the progeny of a single highly-fecund dysgenic F1 mother designated 5011. The
562 mitotic recombination event identified is visible and identifiable in the genotypes of the BC1

563 progeny of F1 mother 5011 in comparison to the BC1 progeny of another high fecundity
564 dysgenic female (4029) that lacks a cluster of recombination in this region (Figure 4A-B).
565 Reciprocal CO products were observed with equal frequency among the BC1 progeny of F1
566 mother 5011 ($\chi^2_1 = 0.13$, $p = 0.727$, Figure 4B) indicating no transmission bias among
567 recombinant gametes. Additional unique COs were detected along the entire length of the third
568 chromosome upstream and downstream of the recombination cluster. The high frequency of
569 recombinants at the same location identified among this cohort of BC1 progeny likely indicates
570 an event in the early germline of the F1 female 5011.
571
572 Another recombination cluster was identified on the X chromosome, approximately 21.7 Mb
573 from the telomere. In this region, there was an effective recombination rate of 15.7 cM / Mb
574 (Figure 3A, within the circled region). Once again, the vast majority of COs within this 500 kb
575 interval are part of another cluster of recombination attributed to a single highly-fecund dysgenic
576 F1 female designated 4029 (Figure 4C). The cluster of recombination is revealed in only half of
577 the progeny of the F1 mother 4029. Interestingly, no additional COs were detected in the portion
578 of the X chromosome distal from the recombination event and all markers in the distal portion
579 were heterozygous. The extreme excess of heterozygosity on the X chromosome in the BC1
580 progeny indicates transmission distortion of the strain 160 genotype distal from the CO from the
581 4029 mother ($\chi^2_1 = 32$, $p = 0.141E-08$, Figure 4C). Markers proximal to the cluster of
582 recombination show no transmission distortion ($\chi^2_1 = 0.13$, $p = 0.727$, Figure 4C). Moreover,
583 crossing over was found to occur in the proximal portion of the X. Thus, it appears that there was
584 germline loss of heterozygosity (LOH) for the distal region of the chromosome in the germline
585 of mother 4029.

586

587 These two clusters of recombination were identified based on their observed higher rates of
588 recombination in the dysgenic germline. We infer the clusters are mitotic recombination hotspots
589 because the chromosomes with the focal recombination event were exclusively found to be
590 derived from a single F1 mother. Additional mitotic COs may be indistinguishable from meiotic
591 recombination since such events may be rare and are only evident if the events occur early
592 enough in development and are associated with depletion of other non-CO germline stem cells.
593 To uncover additional evidence for other mitotic COs in our data, we screened for clusters of
594 recombination by identifying CO events within the same 100 kb interval in four or more progeny
595 of a single F1 mother. Using these criteria, we identified five additional candidate mitotic
596 recombination clusters in progeny from dysgenic mothers and one additional candidate in
597 progeny from a non-dysgenic mother (Table 4). Four of these six additional putative clusters of
598 recombination were also associated with segregation distortion of a single genotype in a
599 significant portion of the chromosome and no additional COs detected in the distorted region
600 (Table 4, Figure S3).

601

602 To address whether activation of TEs during dysgenesis played a role in causing clustered
603 mitotic recombination events, we generated a *de novo* PacBio assembly for strain 160 and
604 determined whether regions of the 160 inducer chromosomes where recombination clusters were
605 identified contained intact copies of TEs implicated in hybrid dysgenesis (*Penelope*,
606 *Polyphemus*, *Helena*, *Skippy*, and *Paris*). Active versions of these TEs are absent in strain 9 and
607 their activation during hybrid dysgenesis may induce DNA damage on the 160 chromosome for
608 subsequent repair *via* mitotic recombination. Of these, *Paris* and *Polyphemus* are the most likely

609 associated with chromosome breaks since they are DNA transposons capable of excision. By
610 examining the PacBio assembly of strain 160, we found that five clusters of recombination
611 contained an intact insertion for a TE known to be absent in strain 9 and present in strain 160
612 within the defined boundaries of the CO (Table 4). Three clusters were associated with
613 *Polyphemus* elements in strain 160. One cluster was associated with a *Paris* element and a fifth
614 cluster on chromosome X contained both elements (Table 4). To determine whether mitotic
615 recombination events are directly associated with excision during dysgenesis, we performed PCR
616 and sequencing on original DNA samples used for Illumina genotyping of the BC1 progeny of
617 F1 mother 5011 with primers that flanked the *Polyphemus* insertion on chromosome 3.
618 Examination of the one individual that retained the strain 160 haplotype across the CO
619 breakpoint indicated that even though there was no recombination event for that sample, excision
620 of *Polyphemus* was identified in the lesion left by the tandem site duplication. In four
621 recombinant samples, we confirmed that *Polyphemus* was absent. Recombination events initiated
622 from an excision are expected to be repaired off the non-insertion chromosome and, thus we
623 were not able to find direct evidence of an excision scar in recombinants lacking the *Polyphemus*
624 element. Nonetheless, these results support the conclusion that this particular *Polyphemus*
625 insertion was activated in female 5011 and this was associated with a cluster of mitotic
626 recombination. Overall, our results suggest clusters of recombination occur more frequently in
627 dysgenic relative to non-dysgenic females and often occur in regions containing intact copies of
628 two DNA transposons (*Polyphemus* and *Paris*) associated with hybrid dysgenesis.
629
630 Since we identified multiple mitotic clusters of recombination in dysgenic crosses, we sought to
631 more formally determine whether there was evidence for a statistically significant higher rate of

632 recombination cluster formation in dysgenic females. Since the criteria for identifying a cluster
633 was based on observing four or more individuals with a CO within a given span, it was necessary
634 to account for variation in cohort size. We achieved this by developing a likelihood model where
635 the probability of observing a set of chromosomes providing evidence of a cluster within a
636 cohort was a function of the probability that a mitotic event occurs on that chromosome within
637 an F1 female (α) and the probability of observing that event on a given chromosome (β) among
638 the sequenced progeny. We considered two, three and four parameter models where either α or β
639 would be the same under dysgenesis or non-dysgenesis, or there would be a unique value
640 depending on condition. Using nested likelihood ratio tests, we find support for a three-
641 parameter model with separate β estimates for dysgenic and non-dysgenic mothers and a shared
642 α estimate over the two-parameter model ($\alpha = 0.12$, $\beta_{Dys} = 0.78$, $\beta_{NonDys} = 0.11$, LRT, $\chi^2_1 = 51.6$,
643 $p = 6.92E\text{-}13$, Table S9). Comparing a three-parameter model where α is estimated separately to
644 the two-parameter model is not supported (LRT, $\chi^2_1 = 3.39$, $p = 0.066$, Table S9). Finally, we do
645 not find support for a four-parameter model over the three-parameter model with separate β
646 estimates (LRT, $\chi^2_1 = 1.88$, $p = 0.170$, Table S9). Overall, these results support a similar
647 baseline rate of occurrence of mitotic events in the dysgenic and non-dysgenic germlines.
648 However, the frequency of chromosomes that are transmitted with mitotic damage is greater in
649 the dysgenic germline. Overall, we find evidence that that the total transmission rate of mitotic
650 damage (α * β) is more than six times greater in the dysgenic germline (0.096 mitotic COs per
651 gamete in dysgenic, 0.014 mitotic COs per gamete in non-dysgenic).
652

653 **DISCUSSION**

654 **A high-resolution genetic map of *D. virilis***

655 In this study, we obtained the first high-resolution genetic map of *D. virilis*. Combined with
656 recombination studies in *D. simulans*, *D. mauritiana*, *D. yakuba*, *D. persimilis*, *D. miranda*, *D.*
657 *serrata*, *D. mojavensis*, and others (Evgen'ev 1976; True *et al.* 1996; Takano-Shimizu 2001;
658 Staten *et al.* 2004; Kulathinal *et al.* 2008; Stevison and Noor 2010; Stocker *et al.* 2012;
659 Smukowski Heil *et al.* 2015; Howie *et al.* 2019), our genetic map of *D. virilis* will aid future
660 studies of the evolution of recombination in *Drosophila*. Of note is the high rate of
661 recombination in *D. virilis* in comparison to other species, especially *D. melanogaster*.
662 Recombination rates in species of *Drosophila* frequently peak in the middle of the chromosome
663 arm and decrease towards the centromere and telomere (True *et al.* 1996). However, the
664 distribution of recombination on the second, third, and fourth chromosomes in *D. virilis*
665 resembles a bimodal distribution (Figure 3). The bimodal distribution may be the result of the
666 exceptionally high recombination rates in *D. virilis*. When two or more crossovers on a single
667 chromosome is common, interference preventing CO formation in close proximity would spread
668 COs more evenly along the length of the chromosome.
669

670 **Meiotic recombination in light of hybrid dysgenesis in *D. virilis***

671 This study is one of the few to examine the effects of TE activity on the meiotic recombination
672 landscape, and the first to do so using the hybrid dysgenesis syndrome in *D. virilis*. Results from
673 previous studies of hybrid dysgenesis in *D. melanogaster* were conflicting as some found no
674 effect on female recombination (Hiraizumi 1971; Chaboissier *et al.* 1995) while others found
675 increases in the recombination rate (Kidwell 1977; Broadhead *et al.* 1977; Sved *et al.* 1991) or
676 changes in the distribution of recombination (Slatko 1978; Hiraizumi 1981). In addition to
677 reporting findings using the dysgenic syndrome of a different species, ours is also the first study

678 to investigate the effects of hybrid dysgenesis on recombination using high-throughput
679 genotyping rather than phenotypic markers. This allows a greater insight into the fine-scale
680 changes in recombination rates and distribution that may previously have escaped unnoticed.
681
682 Modulation of recombination by hybrid dysgenesis may occur through different mechanisms.
683 First, mitotic recombination would be directly initiated by double-stranded breaks (DSBs) that
684 arise from either TE insertion or excision. Second, DSBs caused by TE activity could modulate
685 global recombination rates through DNA damage signaling. In support of the first hypothesis, we
686 identified clusters of recombination originating from mitotic CO events in germline stem cells
687 (GSCs) (Figure 5). During hybrid dysgenesis, the damaging effects of transposons are often
688 observed in the germline during early development (Engels and Preston 1979; Niki and Chigusa
689 1986; Sokolova *et al.* 2010). DSBs produced as an outcome of transposition may be repaired by
690 one of several mechanisms including homologous recombination *via* mitotic crossing over. In
691 the case of the cluster of COs on the third chromosome in F1 mother 5011, excision of a
692 *Polyphemus* DNA transposon may have produced a DSB repaired *via* homologous
693 recombination in the mitotic germline, in G1 prior to DNA replication, within a developing GSC
694 (Figure 5A). In this scenario, reciprocal products of the CO would appear in all daughter cells
695 descended from this GSC and reciprocal products would be observed, on average, in equal
696 frequency among gametes. Alternatively, a mitotic CO may have occurred after DNA replication
697 in G2 prior to mitosis in the germline of the 5011 mother (Figure 5B). During mitosis, the
698 chromatids segregated according to Z segregation (Germani *et al.* 2018; Pimpinelli and Ripoll
699 1986) such that reciprocal CO products were transmitted to one daughter cell while the other
700 daughter cell would have received the non-CO chromatids. Other GSCs must have been retained

701 within the 5011 mother because there are several progeny without the common CO product.
702 However, the limited number of progeny lacking either of the reciprocal CO chromatids
703 indicates a depletion of other intact GSCs. We attribute this to an early crisis in GSC survival
704 due to hybrid dysgenesis, followed by re-population of the GSCs from descendants of a single
705 cell carrying the CO chromatids. GSCs marked with the mitotic CO were thus able to recover
706 and rescue fertility after hybrid dysgenesis in the high fecundity female. This is consistent with
707 the observation that hybrid dysgenesis is associated with an early phase of germline depletion
708 (Sokolova *et al.* 2013).
709
710 A second mitotic CO event on the X, with different consequences, likely occurred in the early
711 developing germline of the 4029 mother (Figure 5C). In this case, there was apparent loss-of-
712 heterozygosity (LOH) distal from the CO. This mitotic CO event would have occurred after
713 DNA replication in G2, with a pattern of X segregation (Germani *et al.* 2018; Pimpinelli and
714 Ripoll 1986) resulting in each daughter cell receiving one chromatid with the CO and one
715 without and LOH distal from the CO. This LOH would be responsible for failure to detect
716 additional meiotic COs derived from the homozygous distal region. The complete transmission
717 distortion of the distal region suggests severe depletion of GSCs with the reciprocal mitotic CO
718 products. Again, this is consistent with a severe reduction of GSCs, followed by re-population
719 from even a single GSC and restoration of fertility in the high fecundity female. Interestingly, the
720 bounds of the mitotic CO derived from the 4029 mother do not contain intact dysgenesis-
721 associated TEs nor any other intact TEs in the strain 160 genome. This mitotic CO may therefore
722 have been the product of a new TE insertion in the genome of the 4029 mother. LOH is also
723 observed among several clusters of recombination and most of these clusters are associated with

724 either *Polyphemus* or *Paris* DNA transposons (Table 4, Figure S3). LOH *via* mitotic
725 recombination is observed after DNA damage or chromosomal breakage in cancer cells (Lasko
726 1991) and in yeast recombination studies (Symington *et al.* 2014). The greater number of mitotic
727 recombination events with segregation distortion observed in our data is consistent with previous
728 observations of non-random segregation of chromatids in clonal analysis; chromatids involved in
729 mitotic exchange are more likely to segregate into separate daughter cells (X segregation) than
730 the same daughter cell (Z segregation) in mosaic analyses (Germani *et al.* 2018; Pimpinelli and
731 Ripoll 1986) Likewise, segregation distortion is frequently observed during hybrid dysgenesis
732 (Kidwell and Kidwell 1975; Kidwell *et al.* 1977). Our study therefore links segregation
733 distortion *via* mitotic recombination and subsequent LOH within female germlines as a result of
734 hybrid dysgenesis.
735
736 The observed number of mitotic CO events identified in dysgenic progeny is interesting because
737 the crossing over pathway is least likely to repair non-programmed DSBs (Preston *et al.* 2006).
738 Mitotic COs only account for ~1% of all COs detected in our dataset and contribute minimally to
739 the genetic map length (Figure S4). Interestingly, the mitotic exchange rate is similar to the rates
740 of male recombination under *P* element hybrid dysgenesis (Kidwell *et al.* 1977; Preston *et al.*
741 1996). Other pathways of DNA damage repair including non-homologous end joining and
742 single-strand annealing are probably more common but undetectable in our assay. Rates of
743 mitotic crossing over may also be higher than what we estimated since many mitotic COs would
744 not meet our criteria for classifying candidate clusters because many dysgenic mothers produced
745 fewer than four offspring.
746

747 Overall, despite evidence for the mitotic recombination associated with DNA transposon
748 excision, we found no major differences in the distribution and frequency of meiotic
749 recombination in *D. virilis* under hybrid dysgenesis, suggesting that DNA damage signaling
750 during dysgenesis does not modulate meiotic recombination. The DNA damage response has a
751 critical role in regulating meiotic recombination (Sjöblom and Lähdetie 1996; Lu *et al*. 2010;
752 Joyce *et al.* 2011). DNA damage response regulators such as *p53* and *chk2* also influence the fate
753 of GSCs during hybrid dysgenesis (Tasnim and Kelleher 2018). The incomplete penetrance of
754 hybrid dysgenesis in *D. virilis* may arise from cell to cell variation in the total amount of DNA
755 damage or in stochastic variation in the DNA damage response. However, we found no
756 differences in recombination rates between dysgenic flies with minimal germline atrophy (high
757 fecundity) and severe germline atrophy (low fecundity). This suggests that DNA damage
758 signaling activated by dysgenesis does not modulate meiotic recombination. This is likely due to
759 the fact that most TE activity happens in GSCs during early development (Engels and Preston
760 1979; Sokolova *et al.* 2010). By the onset of meiosis, the harmful effects of TE activity during
761 dysgenesis may have likely subsided. In *D. virilis*, TE suppression is restored by adulthood in
762 dysgenic progeny *via* re-establishment of asymmetric piRNAs and the negative impacts of
763 dysgenesis disappear in subsequent generations (Erwin *et al.* 2015). This suggests that TEs likely
764 produce few DSBs during meiosis in the *D. virilis* hybrid dysgenesis model. We thus conclude
765 that the timing of transposition is an important factor that determines how TEs influence
766 recombination. In the future, it will be worth investigating whether recombination is also robust
767 to transposition that occurs closer to the initiation of meiotic recombination.
768

Acknowledgements

We thank John Kelly, Stuart Macdonald, Michael Evgen'ev, Sergei Funikov, members of the Robert Unckless and Amanda Larracuente labs, and anonymous reviewers for helpful comments and suggestions. Peter Andolfatto and Audrey Lamb provided guidance on the multiplex shotgun genotyping protocol and Annemarie Chilton produced the custom Tn5 enzyme. Enzyme production and development of the library generation protocol was in part supported by NIH R01 OD010974 to Stuart Macdonald (KU) and Tony Long (UC Irvine). We also thank Jennifer Hackett and the University of Kansas Genome Sequencing Core (NIH COBRE P20GM103638) and Christina McHenry and the University of Michigan Advanced Genomics Core for library prep and sequencing. We also thank the KU Center for Research Computing, especially Riley Epperson, and the Georgia Advanced Computing Resource Center for computational resources. This work was supported by the University of Kansas, the University of Georgia, support from COBRE P20GM103638 and NSF Award 1413532 to JB.

783 **REFERENCES**

784 Alonge, M., S. Soyk, S. Ramakrishnan, X. Wang, F. J. Sedlazeck, Z. B. Lippman, and M. C.
785 Schatz, 2019 Fast and accurate reference-guided scaffolding on draft genomes. bioRxiv
786 https://doi.org/10.1101/519637

787 Andolfatto P., D. Davison, D. Erezyilmaz, T. T. Hu, J. Mast, *et al.*, 2011 Multiplexed shotgun
788 genotyping for rapid and efficient genetic mapping. Genome Res. 21: 610–617.

789 Aravin A. A., G. J. Hannon, and J. Brennecke, 2007 The Piwi-piRNA pathway provides an
790 adaptive defense in the transposon arms race. Science 318: 761–764.

791 Bartolomé C., X. Maside, and B. Charlesworth, 2002 On the abundance and distribution of
792 transposable elements in the genome of *Drosophila melanogaster*. Mol. Biol. Evol. 19:
793 926–937.

794 Bates D., M. Mächler, B. Bolker, and S. Walker, 2015 Fitting linear mixed-effects models using
795 lme4. J. Stat. Softw. 67. https://doi.org/10.18637/jss.v067.i01

796 Begun D. J., and C. F. Aquadro, 1992 Levels of naturally occurring DNA polymorphism
797 correlate with recombination rates in *D. melanogaster*. Nature 356: 519–520.

798 Bennetzen J. L., 2000 Transposable element contributions to plant gene and genome evolution,
799 pp. 251–269 in *Plant Molecular Evolution*.

800 Bergman C. M., H. Quesneville, D. Anxolabéhère, M. Ashburner, 2006 Recurrent insertion and
801 duplication generate networks of transposable element sequences in the *Drosophila*
802 *melanogaster* genome. Genome Biol. 7: R112.

803 Bingham P. M., M. G. Kidwell, and G. M. Rubin, 1982 The molecular basis of *P-M* hybrid
804 dysgenesis: the role of the *P* element, a *P*-strain-specific transposon family. Cell 29: 995–
805 1004.

806 Blumenstiel J. P., 2014 Whole genome sequencing in *Drosophila virilis* identifies *Polyphemus*, a
807 recently activated *Tc1*-like transposon with a possible role in hybrid dysgenesis. Mob. DNA
808 5: 6.

809 Bosco G., P. Campbell, J. T. Leiva-Neto, and T. A. Markow, 2007 Analysis of *Drosophila*
810 species genome size and satellite DNA content reveals significant differences among strains
811 as well as between species. Genetics 177: 1277–1290.

812 Brennecke J., C. D. Malone, A. A. Aravin, R. Sachidanandam, A. Stark, *et al.*, 2008 An
813 epigenetic role for maternally inherited piRNAs in transposon silencing. Science 322:
814 1387–1392.

815 Broadhead R. S., J. F. Kidwell, and M. G. Kidwell, 1977 Variation of the recombination fraction
816 in *Drosophila melanogaster* females. J. Hered. 68: 323–326.

817 Broman K. W., and I. Y. Kwak, R/xoi: tools for analyzing crossover interference. Version 0.67-
818 4. https://cran.r-project.org/web/packages/xoi/index.html

819 Broman K. W., and J. L. Weber, 2000 Characterization of human crossover interference. Am. J.
820 Hum. Genet. 66: 1911–1926.

821 Broman K. W., H. Wu, S. Sen, and G. A. Churchill, 2003 R/qtl: QTL mapping in experimental
822 crosses. Bioinformatics 19: 889–890.

823 Brower-Toland B., S. D. Findley, L. Jiang, L. Liu, H. Yin, *et al.*, 2007 *Drosophila* PIWI
824 associates with chromatin and interacts directly with HP1a. Genes Dev. 21: 2300–2311.

825 Bucheton A., R. Paro, H. M. Sang, A. Pelisson, and D. J. Finnegan, 1984 The molecular basis of
826 *I-R* hybrid dysgenesis in *Drosophila melanogaster*: identification, cloning, and properties of
827 the *I* factor. Cell 38: 153–163.

828 Burt A., 2000 Perspective: sex, recombination, and the efficacy of selection--was Weismann
829 right? Evolution 54: 337–351.

830 Cantarel B. L., I. Korf, S. M. C. Robb, G. Parra, E. Ross, *et al.*, 2008 MAKER: an easy-to-use
831 annotation pipeline designed for emerging model organism genomes. Genome Res. 18:
832 188–196.

833 Chaboissier M. C., F. Lemeunier, and A. Bucheton, 1995 *IR* hybrid dysgenesis increases the
834 frequency of recombination in *Drosophila melanogaster*. Genet. Res. 65: 167–174.

835 Chakraborty M., J. G. Baldwin-Brown, A. D. Long, and J. J. Emerson, 2016 Contiguous and
836 accurate de novo assembly of metazoan genomes with modest long read coverage. Nucleic
837 Acids Res. 44: e147.

838 Chen Y., A. Pane, and T. Schüpbach, 2007 *cutoff* and *aubergine* mutations result in
839 retrotransposon upregulation and checkpoint activation in *Drosophila*. Curr. Biol. 17: 637–
840 642.

841 Comeron J. M., R. Ratnappan, and S. Bailin, 2012 The many landscapes of recombination in
842 *Drosophila melanogaster*. PLoS Genet. 8: e1002905.

843 *Drosophila* 12 Genomes Consortium, 2007 Evolution of genes and genomes on the *Drosophila*
844 phylogeny. Nature 450: 203–218.

845 Engels W. R., and C. R. Preston, 1979 Hybrid dysgenesis in *Drosophila melanogaster*: the
846 biology of female and male sterility. Genetics 92: 161–174.

847 Erwin A. A., M. A. Galdos, M. L. Wickersheim, C. C. Harrison, K. D. Marr, *et al.*, 2015 piRNAs
848 are associated with diverse transgenerational effects on gene and transposon expression in a
849 hybrid dysgenic syndrome of *D. virilis*. PLoS Genet. 11: e1005332.

850 Evgen'ev M. B., 1976 The cytogenetic study of crossing over in interspecific hybrids between
851 *Drosophila virilis* and *D. texana*. Genetics 83: 355–360.

852 Evgen'ev M. B., H. Zelentsova, N. Shostak, M. Kozitsina, V. Barskyi, *et al.*, 1997 *Penelope*, a
853 new family of transposable elements and its possible role in hybrid dysgenesis in
854 *Drosophila virilis*. Proc. Natl. Acad. Sci. U. S. A. 94: 196–201.

855 Funikov S. Y., D. A. Kulikova, G. S. Krasnov, A. P. Rezvykh, L. N. Chuvakova, *et al.*, 2018
856 Spontaneous gain of susceptibility suggests a novel mechanism of resistance to hybrid
857 dysgenesis in *Drosophila virilis*. PLoS Genet. 14: e1007400.

858 Gall J. G., and D. D. Atherton, 1974 Satellite DNA sequences in *Drosophila virilis*. Journal of
859 Molecular Biology 85: 633–664.

860 Germani F., C. Bergantinos, and L. A. Johnston, 2018 Mosaic analysis in *Drosophila*. Genetics
861 208: 473–490.

862 Gramates L. S., S. J. Marygold, G. D. Santos, J.-M. Urbano, G. Antonazzo, *et al.*, 2017 FlyBase
863 at 25: looking to the future. Nucleic Acids Res. 45: D663–D671.

864 Gray Y. H., M. M. Tanaka, and J. A. Sved, 1996 *P*-element-induced recombination in
865 *Drosophila melanogaster*: hybrid element insertion. Genetics 144: 1601–1610.

866 Gubenko I. S., and M. B. Evgen'ev, 1984 Cytological and linkage maps of *Drosophila virilis*
867 chromosomes. Genetica 65: 127–139.

868 Gurevich A., V. Saveliev, N. Vyahhi, and G. Tesler, 2013 QUAST: quality assessment tool for
869 genome assemblies. Bioinformatics 29: 1072–1075.

870 Hartmann M., J. Umbanhowar, and J. Sekelsky, 2019 Centromere-proximal meiotic crossovers
871 in *Drosophila melanogaster* are suppressed by both highly-repetitive heterochromatin and
872 the centromere effect. bioRxiv doi: https://doi.org/10.1101/637561

873 Hickey D. A., 1982 Selfish DNA: a sexually-transmitted nuclear parasite. Genetics 101: 519–
874 531.

875 Hiraizumi Y., 1971 Spontaneous recombination in *Drosophila melanogaster* males. Proc. Natl.
876 Acad. Sci. U. S. A. 68: 268–270.

877 Hiraizumi Y., 1981 Heterochromatic recombination in germ cells of *Drosophila melanogaster*
878 females. Genetics 98: 105–114.

879 Housworth E. A., and F. W. Stahl, 2003 Crossover interference in humans. Am. J. Hum. Genet.
880 73: 188–197.

881 Howie J. M., R. Mazzucco, T. Taus, V. Nolte, and C. Schlotterer, 2018 DNA motifs are not
882 general predictors of recombination in two *Drosophila* sister species. Genome Biol Evol 11:
883 1345-1357.

884 Hughes S. E., D. E. Miller, A. L. Miller, and R. Scott Hawley, 2018 Female meiosis: Synapsis,
885 recombination, and segregation in *Drosophila melanogaster*. Genetics 208: 875–908.

886 Huttunen S., J. Aspi, A. Hoikkala, and C. Schlötterer, 2004 QTL analysis of variation in male
887 courtship song characters in *Drosophila virilis*. Heredity 92: 263–269.

888 Isackson D. R., T. K. Johnson, and R. E. Denell, 1981 Hybrid dysgenesis in *Drosophila*: the
889 mechanism of *T-007*-induced male recombination. Mol. Gen. Genet. 184: 539–543.

890 Jensen P. A., J. R. Stuart, M. P. Goodpaster, J. W. Goodman, and M. J. Simmons, 2008 Cytotype
891 regulation of *P* transposable elements in *Drosophila melanogaster*: Repressor polypeptides
892 or piRNAs? Genetics 179: 1785–1793.

893 Joyce E. F., M. Pedersen, S. Tiong, S. K. White-Brown, A. Paul, *et al.*, 2011 Drosophila ATM
894 and ATR have distinct activities in the regulation of meiotic DNA damage and repair. J.
895 Cell Biol. 195: 359–367.

896 Kazazian H. H. Jr, C. Wong, H. Youssoufian, A. F. Scott, D. G. Phillips, *et al.*, 1988
897 Haemophilia A resulting from de novo insertion of *L1* sequences represents a novel
898 mechanism for mutation in man. Nature 332: 164–166.

899 Kidwell M. G., and J. F. Kidwell, 1975 Spontaneous male recombination and mutation in
900 isogenic-derived chromosomes of *Drosophila melanogaster*. J. Hered. 66: 367–375.

Kidwell M. G., 1977 Reciprocal differences in female recombination associated with hybrid dysgenesis in *Drosophila melanogaster*. Genet. Res. 30: 77–88.

Kidwell M. G., J. F. Kidwell, and J. A. Sved, 1977 Hybrid dysgenesis in *Drosophila melanogaster*: A syndrome of aberrant traits including mutation, sterility and male recombination. Genetics 86: 813–833.

Koehler K. E., R. S. Hawley, S. Sherman, and T. Hassold, 1996 Recombination and nondisjunction in humans and flies. Hum. Mol. Genet. 5 Spec No: 1495–1504.

Kong A., D. F. Gudbjartsson, J. Sainz, G. M. Jonsdottir, S. A. Gudjonsson, *et al.*, 2002 A high-resolution recombination map of the human genome. Nat. Genet. 31: 241–247.

Koren S., B. P. Walenz, K. Berlin, J. R. Miller, N. H. Bergman, *et al.*, 2017 Canu: scalable and accurate long-read assembly via adaptive -mer weighting and repeat separation. Genome Res. 27: 722–736.

Kulathinal R. J., S. M. Bennett, C. L. Fitzpatrick, and M. A. F. Noor, 2008 Fine-scale mapping of recombination rate in *Drosophila* refines its correlation to diversity and divergence. Proc. Natl. Acad. Sci. U. S. A. 105: 10051–10056.

Lasko D., 1991 Loss Of Constitutional Heterozygosity In Human Cancer. Annu. Rev. Genet. 25: 281–314.

Lenth R. V., 2016 Least-Squares Means: The R package lsmeans. J. Stat. Softw. 69. https://doi.org/10.18637/jss.v069.i01

920 Le Thomas A., A. K. Rogers, A. Webster, G. K. Marinov, S. E. Liao, *et al.*, 2013 Piwi induces
921 piRNA-guided transcriptional silencing and establishment of a repressive chromatin state.
922 Genes Dev. 27: 390–399.

923 Li H., 2013 Aligning sequence reads, clone sequences and assembly contigs with BWA-MEM.
924 arXiv preprint arXiv.1303.3997.

925 Li H., 2013 Minimap2: pairwise-alignment for nucleotide sequences. Bioinformatics 34: 3094–
926 3100.

927 Lozovskaya E. R., V. S. Scheinker, and M. B. Evgen'ev, 1990 A hybrid dysgenesis syndrome in
928 *Drosophila virilis*. Genetics 126: 619–623.

929 Lu W.-J., J. Chapo, I. Roig, and J. M. Abrams, 2010 Meiotic recombination provokes functional
930 activation of the p53 regulatory network. Science 328: 1278–1281.

931 McCarron M., A. Duttaroy, G. Doughty, and A. Chovnick, 1994 Drosophila *P* element
932 transposase induces male recombination additively and without a requirement for *P* element
933 excision or insertion. Genetics 136: 1013–1023.

934 Mézard C., M. T. Jahns, and M. Grelon, 2015 Where to cross? New insights into the location of
935 meiotic crossovers. Trends Genet. 31: 393–401.

936 Miller D. E., C. B. Smith, N. Y. Kazemi, A. J. Cockrell, A. V. Arvanitakas, *et al.*, 2016 Whole-
937 genome analysis of individual meiotic events in *Drosophila melanogaster* reveals That
938 noncrossover gene conversions are insensitive to interference and the centromere effect.
939 Genetics 203: 159–171.

940 Niki Y., and I. Chigusa, 1986 Developmental analysis of the gonadal sterility of P-M hybrid
941 dysgenesis in *Drosophila melanogaster*. Jpn. J. Genet. 61: 147–156.

942 Petrov D. A., J. L. Schutzman, D. L. Hartl, and E. R. Lozovskaya, 1995 Diverse transposable
943 elements are mobilized in hybrid dysgenesis in *Drosophila virilis*. Proc. Natl. Acad. Sci. U.
944 S. A. 92: 8050–8054.

945 Picelli S., A. K. Björklund, B. Reinius, S. Sagasser, G. Winberg, *et al.*, 2014 Tn5 transposase
946 and tagmentation procedures for massively scaled sequencing projects. Genome Res. 24:
947 2033–2040.

948 Pimpinelli S., and P. Ripoll., 1986 Nonrandom segregation of centromeres following mitotic
949 recombination in *Drosophila melanogaster*. Proc. Natl. Acad. Sci. U. S. A. 83: 3900–3903.

950 Preston C. R., and W. R. Engels, 1996 *P*-element-induced male recombination and gene
951 conversion in *Drosophila*. Genetics 144: 1611–1622.

952 Preston C. R., J. A. Sved, and W. R. Engels, 1996 Flanking duplications and deletions associated
953 with *P*-induced male recombination in *Drosophila*. Genetics 144: 1623–1638.

954 Preston C. R., C. C. Flores, and W. R. Engels, 2006 Differential usage of alternative pathways of
955 double-strand break repair in *Drosophila*. Genetics 172: 1055–1068.

956 Rizzon C., G. Marais, M. Gouy, and C. Biémont, 2002 Recombination rate and the distribution
957 of transposable elements in the *Drosophila melanogaster* genome. Genome Res. 12: 400–
958 407.

959 Santos T. de los, N. Hunter, C. Lee, B. Larkin, J. Loidl, *et al.*, 2003 The Mus81/Mms4
960 endonuclease acts independently of double-Holliday junction resolution to promote a
961 distinct subset of crossovers during meiosis in budding yeast. Genetics 164: 81–94.

962 Schaeffer S. W., A. Bhutkar, B. F. McAllister, M. Matsuda, L. M. Matzkin, *et al.*, 2008 Polytene
963 chromosomal maps of 11 *Drosophila* species: the order of genomic scaffolds inferred from
964 genetic and physical maps. Genetics 179: 1601–1655.

965 Sienski G., D. Dönertas, and J. Brennecke, 2012 Transcriptional silencing of transposons by Piwi
966 and maelstrom and its impact on chromatin state and gene expression. Cell 151: 964–980.

967 Simão F. A., R. M. Waterhouse, P. Ioannidis, E. V. Kriventseva, and E. M. Zdobnov, 2015
968 BUSCO: assessing genome assembly and annotation completeness with single-copy
969 orthologs. Bioinformatics 31: 3210–3212.

970 Sjöblom T., and J. Lähdetie, 1996 Expression of p53 in normal and gamma-irradiated rat testis
971 suggests a role for p53 in meiotic recombination and repair. Oncogene 12: 2499–2505.

972 Slatis H. M., 1955 A reconsideration of the Brown-dominant position effect. Genetics 40: 246–
973 251.

974 Slatko B. E., 1978 Parameters of male and remale recombination influenced by the *T-007* second
975 chromosome in *Drosophila melanogaster*. Genetics 90: 257–276.

976 Slotkin R. K., R. Keith Slotkin, and R. Martienssen, 2007 Transposable elements and the
977 epigenetic regulation of the genome. Nat. Rev. Genet. 8: 272–285.

978 Smukowski Heil C. S., C. Ellison, M. Dubin, and M. A. F. Noor, 2015 Recombining without
979 Hotspots: A Comprehensive Evolutionary Portrait of Recombination in Two Closely
980 Related Species of *Drosophila*. Genome Biol. Evol. 7: 2829–2842.

981 Sokolova M. I., E. S. Zelentsova, N. V. Rozhkov, and M. B. Evgeniev, 2010 Morphologic and
982 molecular manifestations of hybrid dysgenesis in ontogenesis of *Drosophila virilis*. Russ. J.
983 Dev. Biol. 41: 391–393.

984 Sokolova M. I., E. S. Zelentsova, N. G. Shostak, N. V. Rozhkov, and M. B. Evgen'ev, 2013
985 Ontogenetic consequences of dysgenic crosses in *Drosophila virilis*. Int. J. Dev. Biol. 57:
986 731–739.

987 Staten R., S. D. Schully, and M. A. F. Noor, 2004 A microsatellite linkage map of *Drosophila*
988 *mojavensis*. BMC Genet. 5: 12.

989 Stevison L. S., and M. A. F. Noor, 2010 Genetic and evolutionary correlates of fine-scale
990 recombination rate variation in *Drosophila persimilis*. J. Mol. Evol. 71: 332–345.

991 Stocker A. J., B. B. Rusuwa, M. J. Blacket, F. D. Frentiu, M. Sullivan, *et al.*, 2012 Physical and
992 linkage maps for *Drosophila serrata*, a model species for studies of clinal adaptation and
993 sexual selection. G3 2: 287–297.

994 Sved J. A., L. M. Blackman, A. S. Gilchrist, and W. R. Engels, 1991 High levels of
995 recombination induced by homologous *P* elements in *Drosophila melanogaster*. Mol. Gen.
996 Genet. 225: 443–447.

997 Sved J. A., L. M. Blackman, Y. Svoboda, and R. Colless, 1995 Male recombination with single
998 and homologous *P* elements in *Drosophila melanogaster*. Mol. Gen. Genet. 246: 381–386.

999 Symington L. S., R. Rothstein, and M. Lisby, 2014 Mechanisms and regulation of mitotic
1000 recombination in *Saccharomyces cerevisiae*. Genetics 198: 795–835.

1001 Takano-Shimizu T., 2001 Local changes in GC/AT substitution biases and in crossover
1002 frequencies on *Drosophila* chromosomes. Mol. Biol. Evol. 18: 606–619.

1003 Tarailo-Graovac M., and N. Chen, 2009 Using RepeatMasker to identify repetitive elements in
1004 genomic sequences. Curr Protoc Bioinformatics 25: 4.10.1-4.10.14.

1005 Tasnim S., and E. S. Kelleher, 2018 p53 is required for female germline stem cell maintenance in
1006 *P*-element hybrid dysgenesis. Dev. Biol. 434: 215–220.

1007 True J. R., J. M. Mercer, and C. C. Laurie, 1996 Differences in crossover frequency and
1008 distribution among three sibling species of *Drosophila*. Genetics 142: 507–523.

1009 Vieira J., C. P. Vieira, D. L. Hartl, and E. R. Lozovskaya, 1998 Factors contributing to the hybrid
1010 dysgenesis syndrome in *Drosophila virilis*. Genet. Res. 71: 109–117.

1011 Walker B. J., T. Abeel, T. Shea, M. Priest, A. Abouelliel, *et al.*, 2014 Pilon: an integrated tool for
1012 comprehensive microbial variant detection and genome assembly improvement. PLoS One
1013 9: e112963.

1014 Weinstein A., 1918 Coincidence of crossing over in *Drosophila melanogaster* (*Ampelophila*).
1015 Genetics 3: 135–172.

1016 Weinstein A., 1920 Homologous genes and linear linkage in *Drosophila virilis*. Proc. Natl. Acad.
1017 Sci. U. S. A. 6: 625–639.

1018 Weismann A., J. Arthur Thomson, and M. R. Thomson, 1904 *The evolution theory*.

1019 Westphal T., and G. Reuter, 2002 Recombinogenic effects of suppressors of position-effect
1020 variegation in *Drosophila*. Genetics 160: 609–621.

1021 Wickham H., 2016 *ggplot2: Elegant Graphics for Data Analysis*. Springer.

1022 Wylie A., W.-J. Lu, A. D'Brot, M. Buszczak, and J. M. Abrams, 2014 p53 activity is selectively
1023 licensed in the *Drosophila* stem cell compartment. Elife 3: e01530.

1024 Yannopoulos G., N. Stamatis, M. Monastirioti, P. Hatzopoulos, and C. Louis, 1987 *hobo* is
1025 responsible for the induction of hybrid dysgenesis by strains of *Drosophila melanogaster*
1026 bearing the male recombination factor 23.5MRF. Cell 49: 487–495.

1027 Zdobnov E. M., F. Tegenfeldt, D. Kuznetsov, R. M. Waterhouse, F. A. Simão, *et al.*, 2016
1028 OrthoDb v9.1: cataloging evolutionary and funcational annotations for animal, fungal,
1029 plant, archaeal, bacterial, and viral orthologs. Nucleic Acids Res 45: D744–D749.

1030 Zhang J., C. Yu, L. Krishnaswamy, and T. Peterson, 2011 Transposable elements as catalysts for
1031 chromosome rearrangements. Methods Mol. Biol. 701: 315–326.

1032 Zwick M. E., D. J. Cutler, and C. H. Langley, 1999 Classic Weinstein: tetrad analysis, genetic
1033 variation and achiasmate segregation in *Drosophila* and humans. Genetics 152: 1615–1629.

1034 **TABLES**

1035 **Table 1:** Genetic map lengths of *D. virilis* chromosomes in centiMorgans reported in previous

1036 studies and this study.

	Chromosome					
	X	**2**	**3**	**4**	**5**	**6**
Gubenko & Evgen'ev (1984)	170	257	145	108	203	1
Huttunen *et al.* (2004)	–	118	125	147	60	–
Current study	143.5	160.9	139.6	148.3	140.0	–

1037

1038 **Table 2:** Interference values (*nu*) and frequency of crossovers created in the non-interference

1039 pathway (*P*) for all chromosomes. Both values were estimated with the Housworth-Stahl model

1040 for the entire dataset.

	Chromosome				
	X	**2**	**3**	**4**	**5**
Nu	3.22	3.17	2.68	3.09	3.37
P	4.81E-02	1.05E-02	2.73E-08	6.91E-03	9.75E-03

1041

1042 **Table 3:** Pearson's correlation coeffecients (*R*) and *p*-values between rates of recombination and

1043 sequence parameters calculated in 250 kb intervals.

Sequence Parameter		Chromosome					Total	Total minus Zero CO
		X	2	3	4	5		
GC Content	R	0.08	0.35	0.11	0.18	0.33	0.23	0.15
	p	0.372	<0.001	0.263	0.079	<0.001	<0.001	<0.001
Gene density	R	0.31	0.21	0.12	0.32	0.33	0.19	0.03
	p	<0.001	0.012	0.222	<0.001	<0.001	<0.001	0.506
Simple repeats	R	0.44	0.43	0.31	0.32	0.54	0.39	0.177
	p	<0.001	<0.001	<0.001	<0.001	<0.001	<1E-10	<0.001
SNP Density	R	0.64	0.553	0.60	0.67	0.65	0.62	0.49
	p	<1E-10	<1E-10	<1E-10	<1E-10	<1E-10	<1E-10	<1E-10
TE Density	R	-0.47	-0.47	-0.33	-0.44	-0.49	-0.44	-0.14
	p	<0.001	<0.001	<0.001	<0.001	<0.001	<1E-10	<0.001

1044

1045 **Table 4:** Clusters of recombination identified in the BC1 progeny.

F1 Female Identifier	Chromosome	Position (Mb from Telomere)	CO Progeny / Total Progeny	Distortion Genotype	TEs detected in Strain 160
3*	X	17.7	4 / 29	None	*Polyphemus*
111	3	25.1	4 / 11	Strain 9**	*Polyphemus*
4013	X	11.4	4 / 13	Strain 160	None
4029	X	21.3	14 / 19	Strain 160	None
5011	3	9.8	28 / 32	None	*Polyphemus*
5019	3	20.2	10 / 30	Strain 9**	None
5022	3	23.6	5 / 11	Strain 9**	*Paris*
5089	X	23.4	4 / 11	Strain 160	*Polyphemus* x2, Paris

1046

1047 * The F1 female is non-dysgenic

1048 ** Segregation distortion occurred in some of the progeny. The rest appear normal and probably

1049 did not inherit a mitotic CO chromatid

1050 **FIGURES**

1051 **Figure 1:** The distribution of the total crossover (CO) count observed in individual BC1 progeny
1052 with the mean and standard deviation. The mean for each group is represented with a black dot
1053 and the standard deviation is the black line. A) The distribution of the total CO count per BC1
1054 progeny of low fecundity dysgenic, high fecundity and non-dysgenic F1 mothers. B) The
1055 distribution of CO count per BC1 progeny of each high fecundity dysgenic mother with mean
1056 and standard deviation. Asterisks denotes statistical significance by least square means ($p <$
1057 0.05). Progeny from mother 701 had a higher average CO count than progeny from other
1058 mothers while progeny from mother 4029 exhibited a lower average CO count.

1059

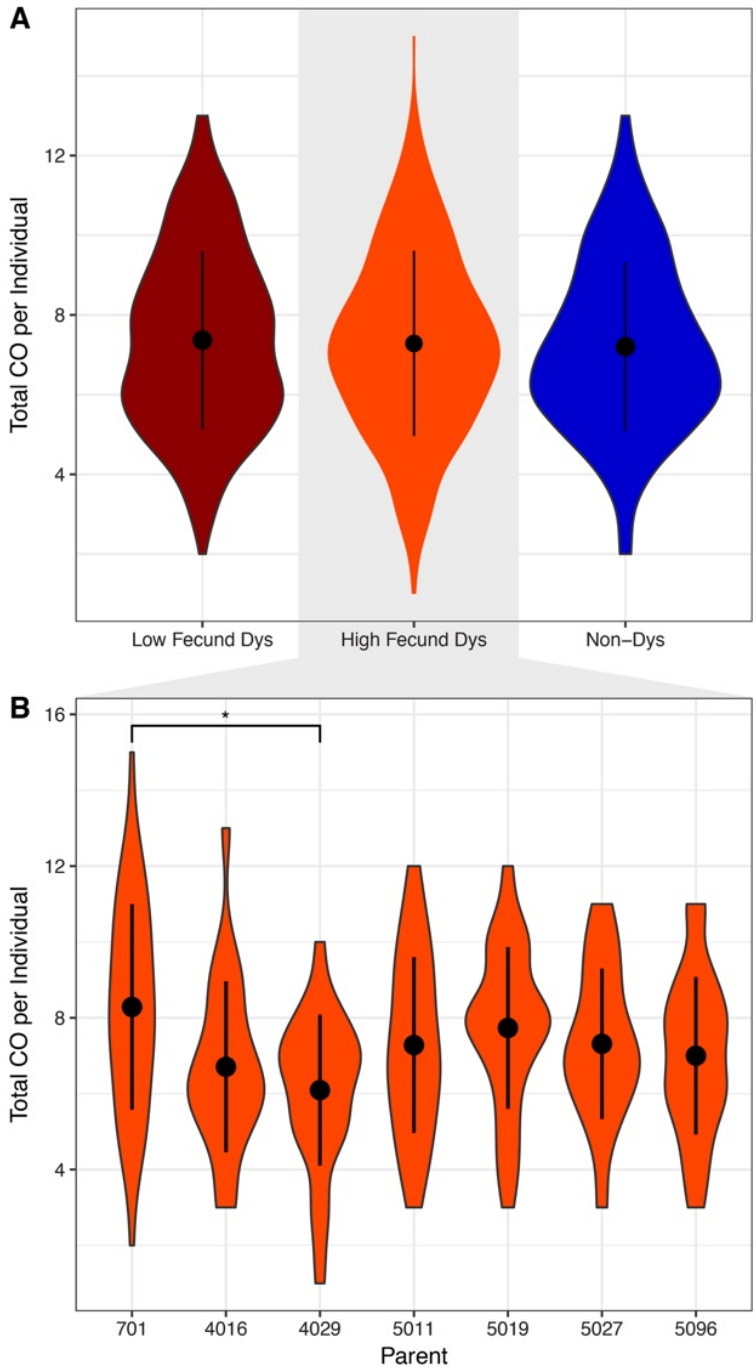
A
Total CO per Individual
12
8
4
Low Fecund Dys
High Fecund Dys
Non−Dys
B
16
12
8
4
*
701
4016
4029
5011
5019
5027
5096
Parent

1060

1061 **Figure 2:** The proportion of chromosomes grouped by CO count in BC1 progeny of high fecund

1062 dysgenic, low fecund dysgenic, and non-dysgenic F1 mothers. 95% confidence intervals were

1063 calculated by sampling BC1 progeny by bootstrapping 1000 times.

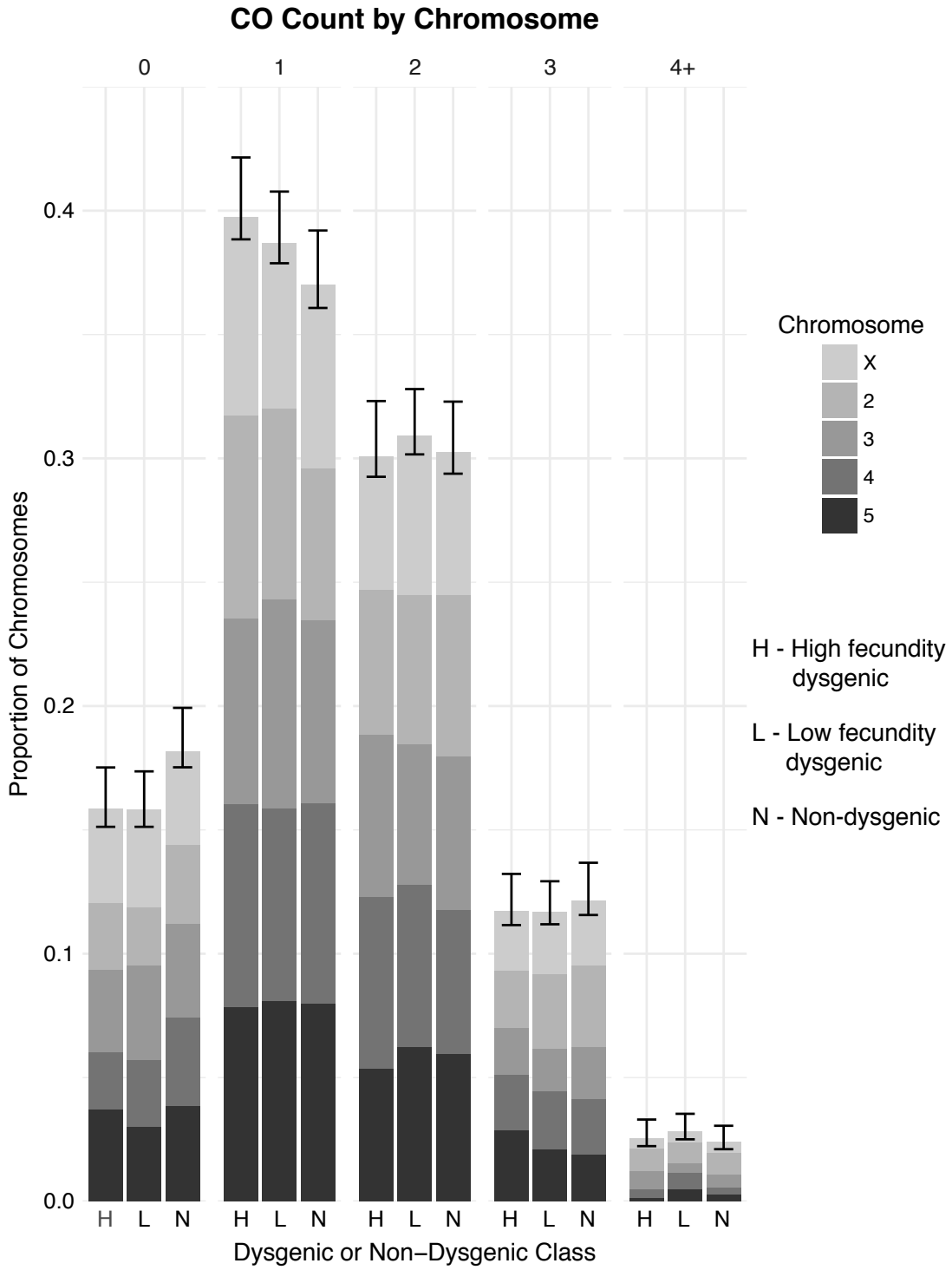

1064

1065 **Figure 3:** Loess smoothed splines of the recombination rate along the length of each
1066 chromosome in *D. virilis* from the telomere (left) to the centromere (right) with standard error.
1067 The dotted line represents the centromere effect of recombination suppression as recombination
1068 = 0 from the line to the end of the sequence. The rate of recombination was calculated in 500 kb
1069 intervals in F2 progeny of low fecund dysgenic, high fecund and non-dysgenic F1 mothers for
1070 the A) X chromosome, B) 2nd chromosome, C) 3rd chromosome, D) 4th chromosome, and E)
1071 5th chromosome.

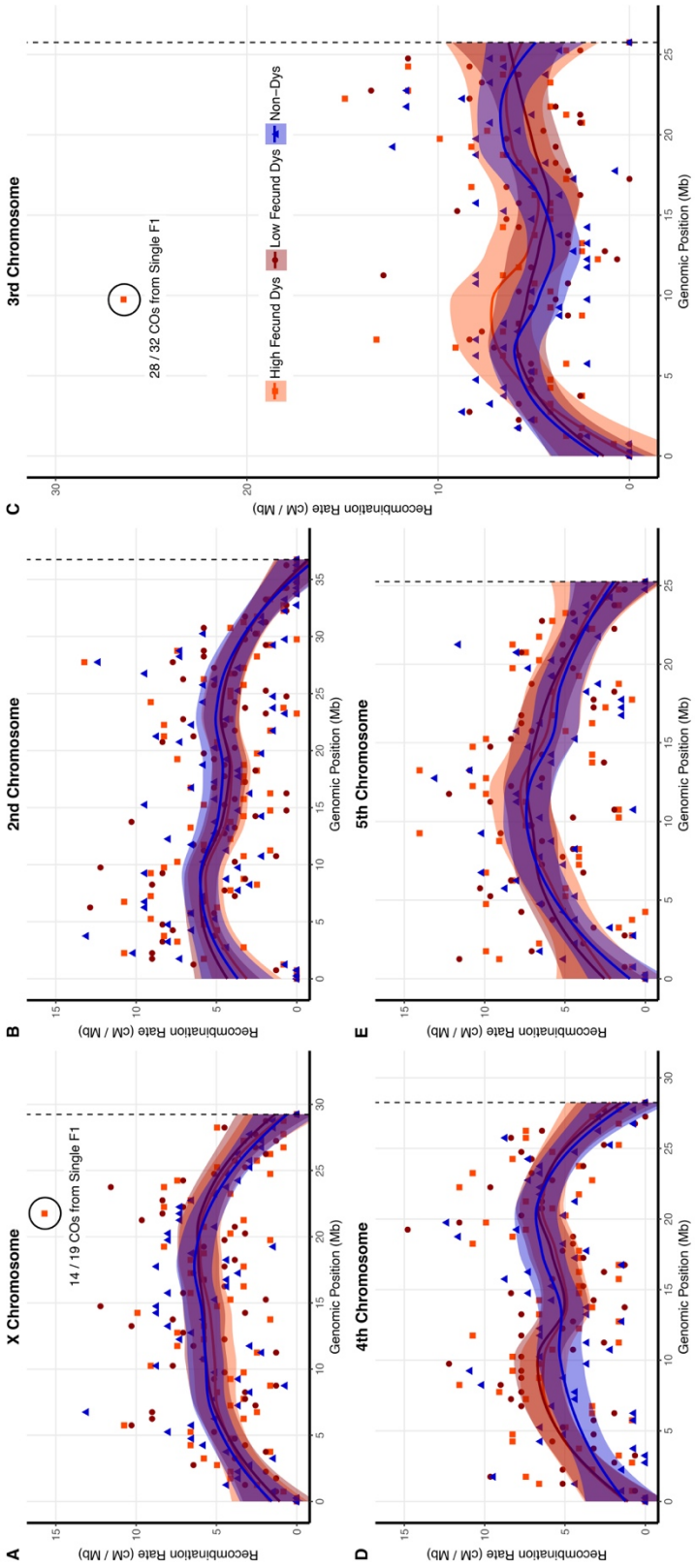
A
X Chromosome
14 / 19 COs from Single F1
Recombination Rate (cM / Mb)
Genomic Position (Mb)
B
2nd Chromosome
Recombination Rate (cM / Mb)
Genomic Position (Mb)
C
3rd Chromosome
28 / 32 COs from Single F1
High Fecund Dys
Low Fecund Dys
Non−Dys
Recombination Rate (cM / Mb)
Genomic Position (Mb)
D
4th Chromosome
Recombination Rate (cM / Mb)
Genomic Position (Mb)
E
5th Chromosome
Recombination Rate (cM / Mb)
Genomic Position (Mb)

1074 **Figure 4:** Haplotypes of BC1 progeny from a single high-fecund dysgenic mother. A)
1075 Haplotypes of the third chromosome in progeny of the 4029 F1 mother is typical of most
1076 chromosomes with no cluster of recombination. B) Haplotypes of the third chromosome in
1077 progeny of the 5011 F1 mother identify a common recombination breakpoint in most of the
1078 progeny and reciprocal products of recombination in equal frequency (Binomial test, $p > 0.05$).
1079 C) Haplotypes of the X chromosome in progeny of the 4029 F1 mother indicate a common
1080 recombination breakpoint in half of the progeny and extreme segregation distortion of the distal
1081 portion of the chromosome (227 markers 0.5 - 21.4 MB, Binomial test, $p < 1.6E-08$). The
1082 proximal region of the chromosome shows no segregation distortion (86 markers 21.5 - 29.0 Mb
1083 Binomial test, $p > 0.5$).

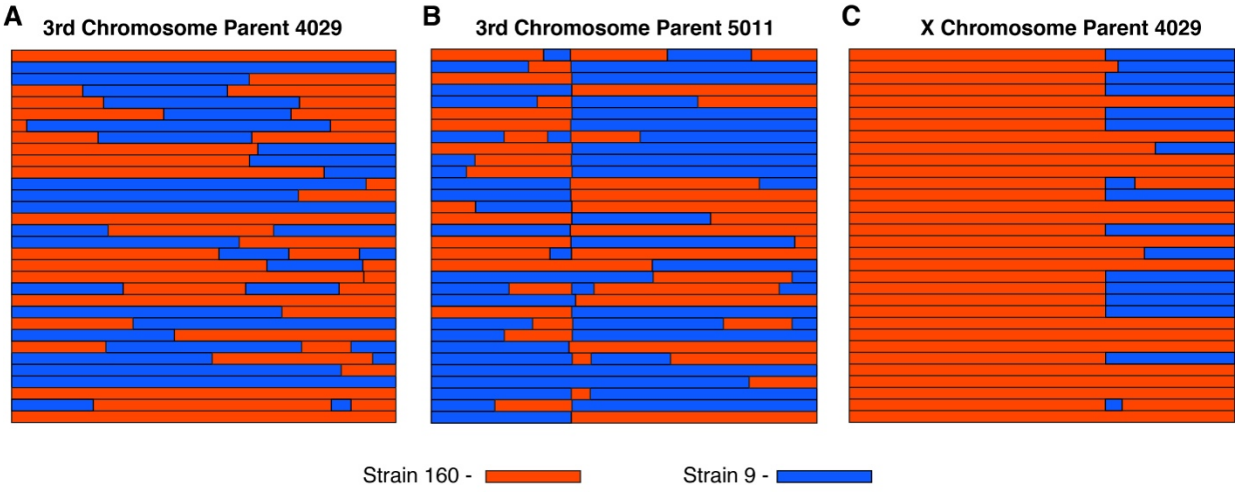

1084
1085

1086 **Figure 5:** Models to explain the clusters of recombination on the third and X chromosomes in
1087 the progeny of two high fecundity dysgenic mothers. In the 5011 F1 female, a mitotic crossover
1088 (CO) either occurred A) prior to DNA replication in the early developing germline resulting in
1089 two daughter cells with the CO or B) after DNA replication, followed by a pattern of Z
1090 segregation so that one daughter cell has both CO chromatids. Oocytes produced by these
1091 germline stem cells will transmit the CO as reciprocal products as seen if the CO occurred in G1.
1092 C) A mitotic CO in the 4029 F1 female occurred after DNA replication in the developing
1093 germline and each daughter cell received one CO chromatid and one non-CO chromatid
1094 according to a pattern of X segregation. This results in a loss of heterozygosity (LOH) in the
1095 distal portion of the chromosome to resemble segregation distortion and recombination events
1096 are not detectable.
1097

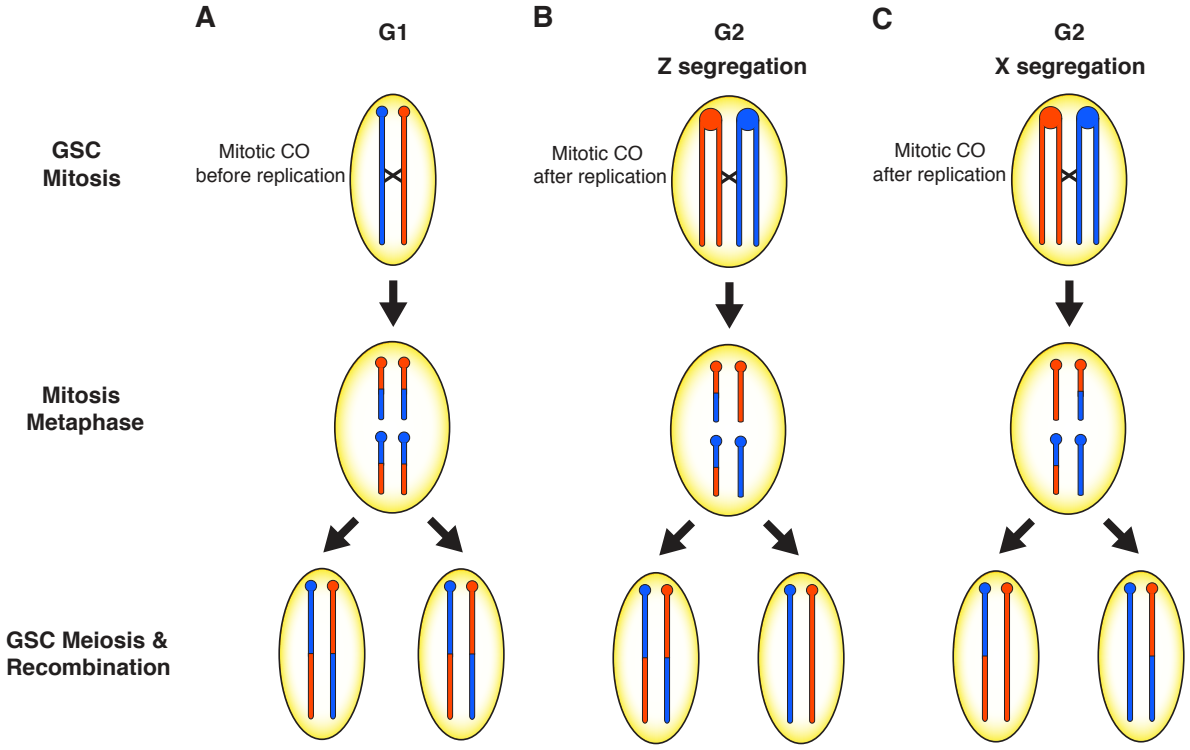
A
G1
B
G2
Z segregation
C
G2
X segregation
GSC
Mitosis
Mitotic CO
before replication
Mitotic CO
after replication
Mitotic CO
after replication
Mitosis
Metaphase
GSC Meiosis &
Recombination

1098